Geosphere

Chronology of Eocene–Miocene sequences on the New Jersey shallow shelf: Implications for regional, interregional, and global correlations

James V. Browning, Kenneth G. Miller, Peter J. Sugarman, John Barron, Francine M.G. McCarthy, Denise K. Kulhanek, Miriam E. Katz and Mark D. Feigenson

Geosphere published online 11 October 2013;
doi: 10.1130/GES00857.1

Notes

Chronology of Eocene–Miocene sequences on the New Jersey shallow shelf: Implications for regional, interregional, and global correlations

James V. Browning[1], Kenneth G. Miller[1], Peter J. Sugarman[1], John Barron[2], Francine M.G. McCarthy[3], Denise K. Kulhanek[4,*], Miriam E. Katz[5], and Mark D. Feigenson[1]

[1]*Department of Earth and Planetary Sciences, Rutgers University, Piscataway, New Jersey 08854, USA*
[2]*U.S. Geological Survey, MS 910, Menlo Park, California 94025, USA*
[3]*Department of Earth Sciences, Brock University, St. Catharines, ONT L2S 3A1, Canada*
[4]*GNS Science, Department of Paleontology, PO Box 30368, Lower Hutt 5040, New Zealand*
[5]*Earth & Environmental Sciences, Rensselaer Polytechnic Institute, Troy, New York 12180, USA*

ABSTRACT

Integrated Ocean Drilling Program Expedition 313 continuously cored and logged latest Eocene to early-middle Miocene sequences at three sites (M27, M28, and M29) on the inner-middle continental shelf offshore New Jersey, providing an opportunity to evaluate the ages, global correlations, and significance of sequence boundaries. We provide a chronology for these sequences using integrated strontium isotopic stratigraphy and biostratigraphy (primarily calcareous nannoplankton, diatoms, and dinocysts [dinoflagellate cysts]). Despite challenges posed by shallow-water sediments, age resolution is typically ±0.5 m.y. and in many sequences is as good as ±0.25 m.y. Three Oligocene sequences were sampled at Site M27 on sequence bottomsets. Fifteen early to early-middle Miocene sequences were dated at Sites M27, M28, and M29 across clinothems in topsets, foresets (where the sequences are thickest), and bottomsets. A few sequences have coarse (~1 m.y.) or little age constraint due to barren zones; we constrain the age estimates of these less well dated sequences by applying the principle of superposition, i.e., sediments above sequence boundaries in any site are younger than the sediments below the sequence boundaries at other sites. Our age control provides constraints on the timing of deposition in the clinothem; sequences on the topsets are generally the youngest in the clinothem, whereas the bottomsets generally are the oldest. The greatest amount of time is represented on foresets, although we have no evidence for a correlative conformity. Our chronology provides a baseline for regional and interregional correlations and sea-level reconstructions: (1) we correlate a major increase in sedimentation rate precisely with the timing of the middle Miocene climate changes associated with the development of a permanent East Antarctic Ice Sheet; and (2) the timing of sequence boundaries matches the deep-sea oxygen isotopic record, implicating glacioeustasy as a major driver for forming sequence boundaries.

INTRODUCTION

Integrated Ocean Drilling Program (IODP) Expedition 313 drilled the New Jersey shallow continental shelf to evaluate development of sequences (unconformity-bounded units) on a passive continental margin (Mountain et al., 2010). The formation of sequence-bounding regional unconformities has been attributed primarily to tectonism (basin subsidence and uplift; e.g., Embry, 2009) and/or eustasy (global sea-level change; e.g., Vail et al., 1977), with sediment supply playing a minimal role in their formation (Christie-Blick et al., 1990). Several previous studies documented early to middle Miocene sequence boundaries on multichannel seismic (MCS) profiles across the shallow continental shelf off New Jersey (Greenlee and Moore, 1988; Greenlee et al., 1992; Monteverde, 2008; Monteverde et al., 2008; Mountain et al., 2010). The seismic arrays afforded by these generations of site surveys (Fig. 1) allowed planning a transect of coreholes across the New Jersey coastal plain, shelf, and slope to evaluate the controls on depositional sequences. Ocean Drilling Program (ODP) Leg 150 (Mountain et al., 1996) drilled the continental slope, ODP Leg 174A (Austin et al., 1998) drilled the slope and outer shelf, and ODP Legs 150X and 174AX (Miller et al., 2003) drilled the onshore coastal plain. Sequences beneath the inner continental shelf contain Miocene facies most sensitive to sea-level changes (shoreface to middle neritic environments), but were poorly sampled before Expedition 313.

Sequence boundaries are recognized on MCS profiles beneath the inner to middle continental shelf offshore New Jersey by geometries of onlap, erosional truncation, downlap, and toplap (Monteverde et al., 2008: Mountain et al., 2010). Prograding Miocene clinoform seismic geometries were first recognized on the Atlantic margin as deltas on U.S. Geological Survey reconnaissance MCS profiles (Schlee, 1981; summary in Poag, 1985), but are now recognized as clinothems, packages of sediment that prograde seaward into deeper water bounded by surfaces (in this case sequence boundaries) with distinct sigmoidal (clinoform) shape. The thickest part of the clinoform, the foreset, is found where there is a change in slope from flatter (~1:1000) landward to steeper (~1:500) seaward. Beds preserved landward of the clinoform are known as topset beds and those preserved seaward of the clinoform are known as bottomset deposits (Mountain et al., 2010; Fig. 2).

Previous studies suggested a link between the timing of sequence boundaries on the New Jersey margin and deep-sea benthic foraminiferal $\delta^{18}O$ increases. In Miller et al. (1996, 1997), a chronology for Eocene–Miocene sequences drilled onshore New Jersey (Leg 150X) and on the continental slope (Leg 150) was provided, and the ages of sequence boundaries were compared to the $\delta^{18}O$ proxy of ice growth; a match was found between the timing and number of middle Eocene to Miocene sequence boundaries and $\delta^{18}O$ increases, and it was concluded that growth of ice sheets was the major cause

*Present address: Integrated Ocean Drilling Program, Texas A&M University, 1000 Discovery Drive, College Station, Texas 77845, USA

Geosphere; December 2013; v. 9; no. 6; doi:10.1130/GES00857.1; 7 figures; 2 tables; 1 supplemental figure.
Received 8 August 2012 ♦ Revision received 18 June 2013 ♦ Accepted 19 August 2013 ♦ Published online 11 October 2013

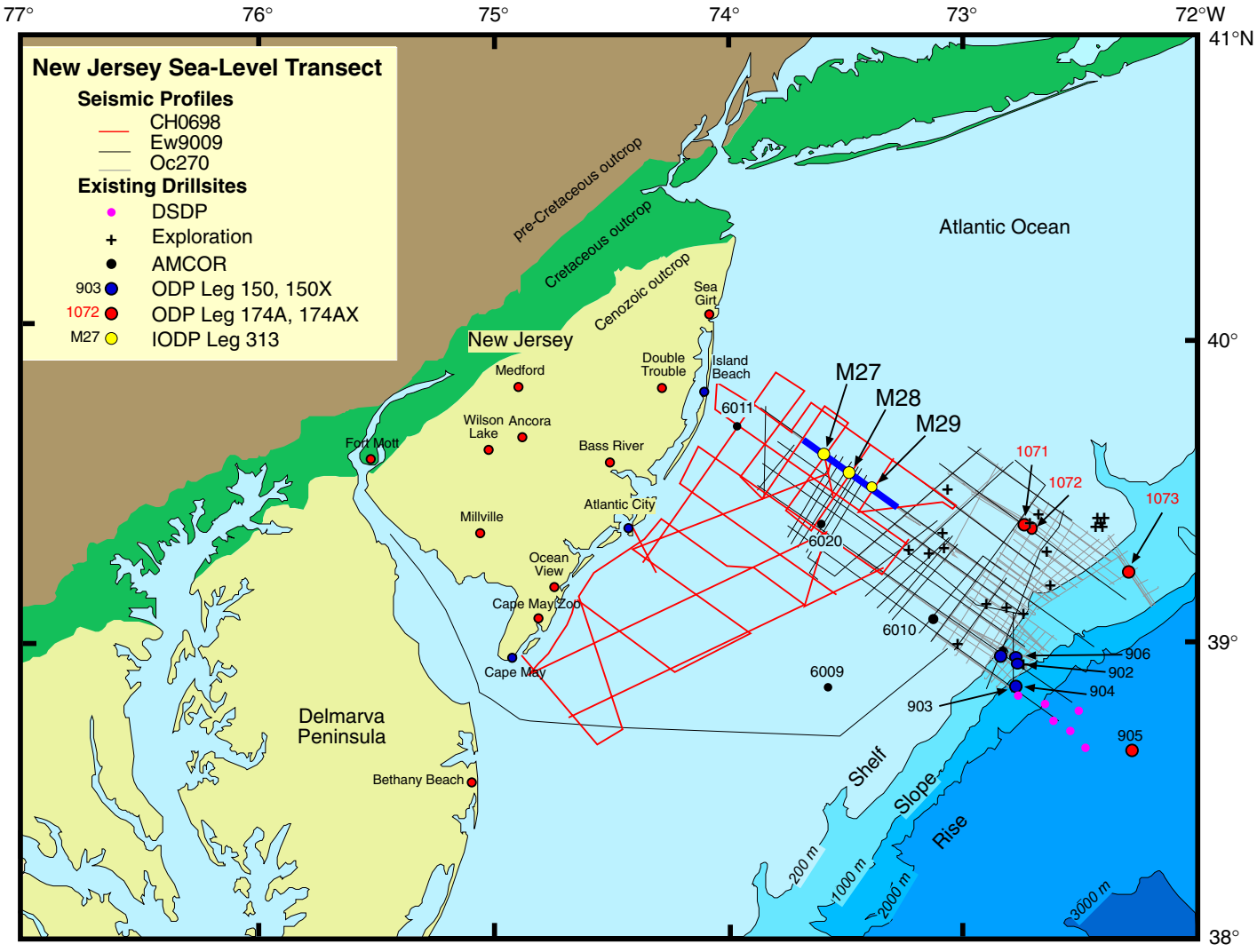

Figure 1. Generalized bathymetric location map of the New Jersey–Mid Atlantic Margin sea-level transect showing track lines for three generations of multichannel seismic data (R/V *Ewing* cruise Ew9009, R/V *Oceanus* cruise Oc270, and R/V *Cape Hatteras* cruise CH0698), onshore coreholes, and offshore coreholes drilled by the Atlantic Margin Coring Project (AMCOR; Hathaway et al., 1979), the Ocean Drilling Program (ODP), and the Integrated Ocean Drilling Program (IODP). DSDP—Deep Sea Drilling Project. Heavy blue line indicates location of OC270 Line 529 in Fig. 2.

of sequence boundaries. However, correlation of onshore Miocene sequences was limited by relatively coarse age control (±1 m.y.), lack of seismic profiles onshore, and highly truncated Miocene sequences due to their location on updip topsets. Expedition 313 sampled early to early-middle Miocene sequences that address these limitations.

Expedition 313 completed the New Jersey sea-level transect by drilling well-imaged seismic sequences beneath the modern inner to middle continental shelf off New Jersey (Monteverde et al., 2008; Mountain et al., 2010) to evaluate their environments of deposition, age relations, and potential controls. It focused on continuously coring early to middle Miocene sequences that were deposited during an icehouse interval when the growth and decay of large ice sheets on Antarctica drove glacio-eustatic changes (e.g., Miller et al., 1991b; Zachos et al., 2001). Three sites (M27–M29; Fig. 1) were cored and logged on a dip transect, recovering Eocene to Holocene sequences in April to July 2009 (Mountain et al., 2010). Fifteen early to middle Miocene sequence boundaries were recognized on seismic profiles and correlated to the Expedition 313 sites using a velocity-depth function (Mountain et al., 2010). Sequence boundaries were also recognized in the Expedition 313 cores using physical stratigraphy and subsequently correlated with the seismic sequences using synthetic seismograms and a revised velocity-depth function (Mountain and Monteverde, 2012; Miller et al., 2013b). Here we develop a chronology for these shallow-water (inner-middle neritic) sequences, which can then be used for interregional correlations including proxies for eustasy, particularly $\delta^{18}O$ records (e.g., Miller et al., 1997, 2005).

Developing a chronology of sediments deposited in a nearshore setting such as those recovered by Expedition 313 is challenging. Nearshore sediments are generally sandy and are thus often unsuitable for magnetostratigraphic studies. Biostratigraphy can also be challenging in nearshore sediments because open-ocean plankton are often excluded in shallow water, making zonation difficult. Expedition 313 was

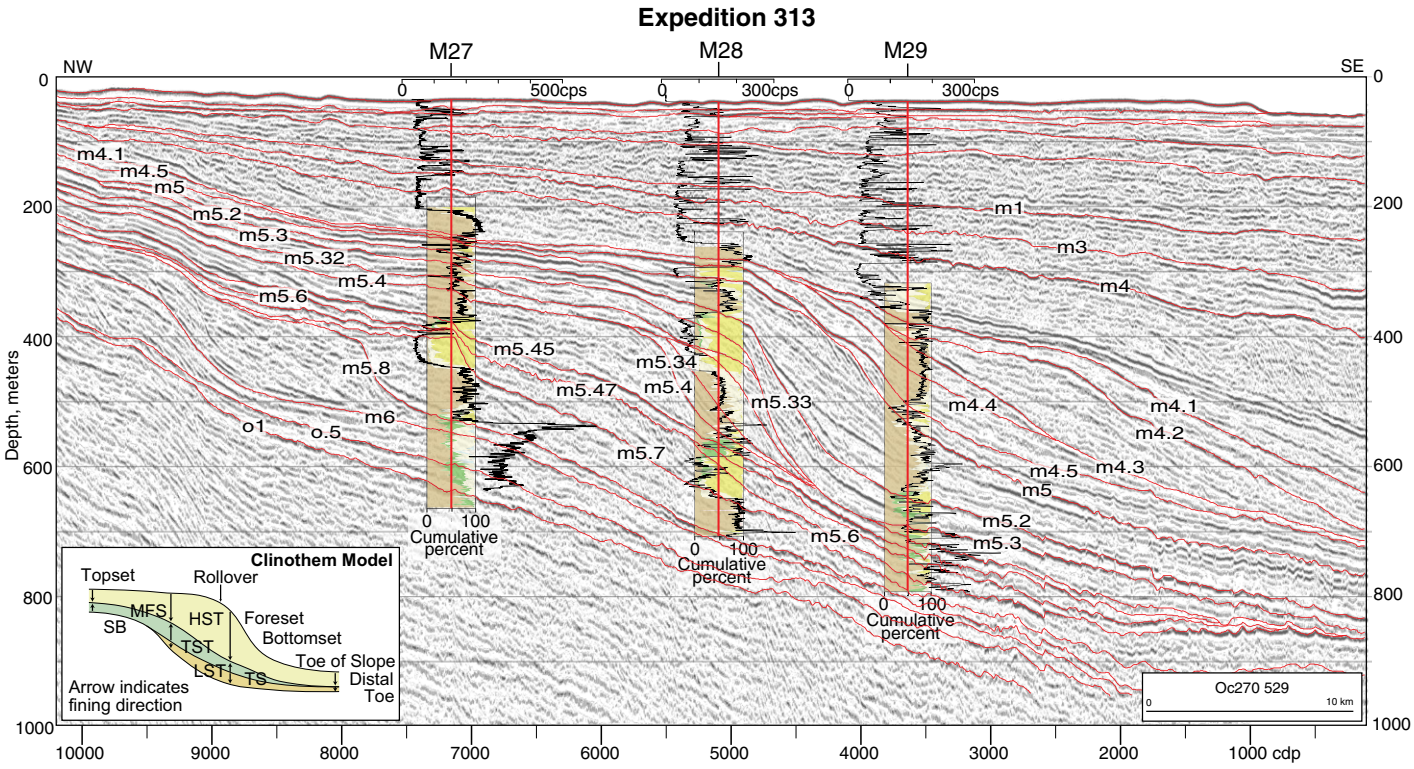

Figure 2. Multichannel seismic profile Oc270 (R/V *Oceanus* cruise 529) trending northwest to southeast to across Integrated Ocean Drilling Program Expedition 313 Sites M27–M29. Traveltime has been converted to depth below sea level (Mountain and Monteverde, 2012). Major seismic sequence boundaries (SB) and select intrasequence reflectors (o.1, o.5, m5.33) are shown; all others are seismic sequence boundaries (m4.1 is a merged transgressive surface [TS] and sequence boundary in this area). Grain size estimates (in cumulative percent; see Miller et al., 2013c) and downhole gamma logs (in counts per second, cps) are superimposed at each site location. The key for the colors used in the cumulative percentage plots is in Figure 4. Inset at lower left is a generalized clinothem model after Miller et al. (2013c). LST—lowstand systems tract; HST—highstand systems tract; TST—transgressive systems tract; MFS—maximum flooding surface; cdp—common depth point.

fortunate to have obtained excellent biostratigraphy using calcareous nannoplankton (Kulhanek, *in* Mountain et al., 2010), dinoflagellate cysts (McCarthy et al., 2013), and planktonic diatoms (Barron et al., 2013). Strontium (Sr) isotope stratigraphy can also be a useful tool for dating nearshore sediments (Miller et al., 1998; Sugarman et al., 1993). This approach relies on the changing ratio of $^{87}Sr/^{86}Sr$ isotopes in the world's ocean as a means of correlating to an established change in seawater through time (e.g., Burke et al., 1982). Sr isotopes are useful during intervals when the Sr isotopic ratio changed rapidly, including the early to middle Miocene and to a lesser extent the Oligocene and middle Miocene (Fig. 3; Oslick et al., 1994; Reilly et al., 2002; McArthur et al., 2001).

The goal of this paper is to provide a chronology for Eocene to Miocene strata recovered by Expedition 313 by integrating sequence boundaries identified in Monteverde et al. (2008), Mountain et al. (2010), and Miller et al. (2013b, 2013c) with Sr isotope stratigraphy (this study) and biostratigraphy (Kulhanek, *in* Mountain et al., 2010; McCarthy et al., 2013; Barron et al., 2013). Pleistocene strata are discussed in Miller et al. (2013a) and Pliocene strata were not sampled by Expedition 313. The chronology afforded is generally ±0.5 m.y. or better and allows evaluation of rates of processes. The age control provided here provides a means of evaluating regional (onshore to offshore), interregional, and global correlations (e.g., with the deep-sea $\delta^{18}O$ record). Here we provide correlations of Expedition 313 sequences to an updated global $\delta^{18}O$ compilation that provides a glacioeustatic proxy. Our chronology can be used to place paleoenvironmental reconstructions into a chronologic framework (Miller et al., 2013b; Katz et al., 2013; McCarthy et al., 2013) and to derive a sea-level estimate using backstripping (Kominz et al., 2008).

METHODS

We constructed our chronology using 254 Sr isotopic age estimates (Table 1). We integrated our Sr isotopic age estimates with calcareous nannofossil (Kulhanek, *in* Mountain et al., 2010), diatom (Barron et al., 2013), and dinocyst (dinoflagellate cysts) (McCarthy et al., 2013) biostratigraphy on a series of age-depth diagrams (Figs. 4–6). Expedition 313 cored primarily sands and silts, but even in the finer grained beds, the magnetic signature was not suitable because it was overprinted due to the formation of greigite (Mountain et al., 2010). As a result, it was not possible to construct a magnetochronology for Expedition 313 strata. Planktonic foraminifers were generally rare in Expedition 313 coreholes and usually consisted of long-ranging forms and thus provide few constraints on our age estimates.

Sr Isotopes

Sr isotope stratigraphy relies on measuring carbonate unknowns (calcite or aragonite shells or foraminiferal tests) and obtaining age estimates using the measured $^{87}Sr/^{86}Sr$ values calibrated to a known change in seawater $^{87}Sr/^{86}Sr$ through time. Seawater $^{87}Sr/^{86}Sr$ is uniform

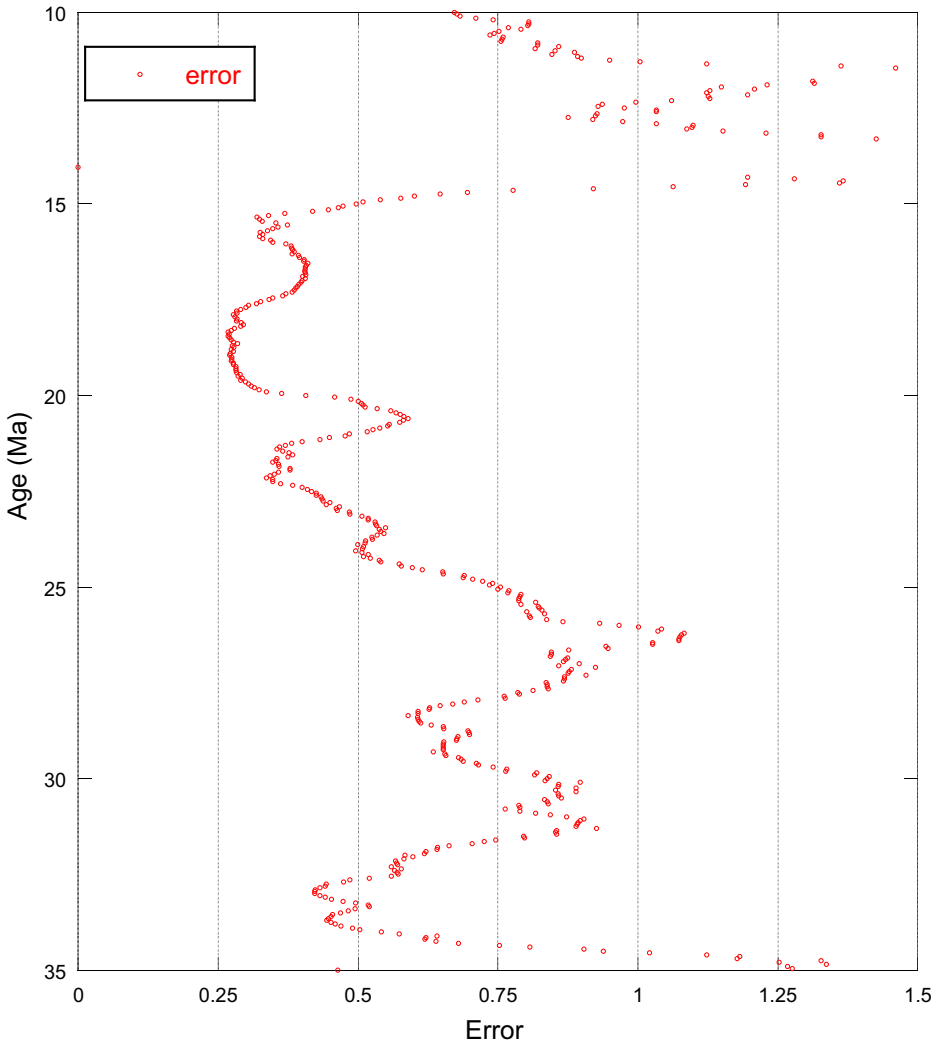

Figure 3. Sr isotopic resolution computed from the compilation of McArthur et al. (2001). We computed total errors using the McArthur et al. (2001) LOWESS (locally weighted scatterplot smoothing) by determining the rate of change of Sr and dividing into an error estimate of 0.000008 (external precision) plus the difference between the upper and lower Sr isotopic estimates (2 σ) for a given level (interpolated to 0.05 m.y. intervals).

throughout the open ocean because the residence time of Sr (~2.5 m.y., Hodell et al., 1990; ~5 m.y., Broecker and Peng, 1982) is much longer than oceanic mixing times (~1 k.y., Broecker and Peng, 1982). Sr substitutes for calcium in the carbonate lattice of inorganically or organically precipitated $CaCO_3$. Because Sr isotopes are approximately the same size as calcium, they are incorporated in carbonate without fractionation. Unaltered carbonate from any marine source, including mollusk shell or foraminiferal test, can be used to determine the ratio of seawater Sr, which can then be interpreted as an age using published calibrations.

Calcium carbonate is a minor component of many Expedition 313 samples (blue on cumulative percent in Figs. 4–6) and thus Sr isotopic age estimates were obtained from mixed species of mollusk shells, shell fragments, and foraminiferal tests (~4–6 mg of $CaCO_3$) in the Expedition 313 coreholes. Analysis of different species and/or genera or even phyla is justified by the fact that no vital effects have been documented for Sr isotopes (Burke et al., 1982). However, diagenesis, stratigraphic reworking, and downslope transport are potential concerns. We generally chose well-preserved calcite, excluding chalky shells or carbonate with inclusions of glauconite or pyrite. We avoided aragonite, which is more easily altered (Sugarman et al., 1995). In the topset sections, downslope transport is a minor issue; in the bottomsets, especially above sequence m5 (Figs. 2 and 4–6), reworking of stratigraphically older material into younger is manifest in the discordant age relations with biostratigraphic age estimates (discussed in the following).

Shells and tests were cleaned ultrasonically and dissolved in 1.5 N HCl. Sr was separated using standard ion-exchange techniques (Hart and Brooks, 1974). The samples were analyzed for $^{87}Sr/^{86}Sr$ on an IsoProbe-T multicollector thermal ionization mass spectrometer and tabulated here (Table 1). Internal (machine) precision on the IsoProbe-T spectrometer for the data set averaged 0.000007 and the external precision is ~±0.000008 (based on replicate analyses of standards). We measured the NBS 987 standard as 0.710243 normalized to $^{86}Sr/^{88}Sr$ of 0.1194 during the period of measurement. Age estimates (Table 1) were derived using the Eocene–Miocene look-up tables of McArthur et al. (2001) recalibrated to the Gradstein et al. (2004) time scale. For Miocene age estimates younger than 15 Ma, we also used a regression of the Oslick et al. (1994) data for ODP Site 747 recalibrated to the Gradstein et al. (2004) time scale (Table 1). Use of the Oslick et al. (1994) regression yielded ages that were closer to biostratigraphic age estimates, although neither regression fit well.

Sr isotope age errors can be derived from linear regressions of Sr isotopic records (Miller et al., 1991a; Oslick et al., 1994; Reilly et al., 2002). Age errors for 15.5–22.8 Ma and 9.7–15.5 Ma are ±0.61 m.y. and ±1.17 m.y., respectively, at the 95% confidence interval for a single analysis based on linear regression (Miller et al., 1991a; Oslick et al., 1994; Reilly et al., 2002). Increasing the number of analyses at a given level improves the age estimate (±0.40 and ±0.76 Ma for three analyses each in the two Miocene intervals; Oslick et al., 1994). Oligocene resolution is ±1.2 m.y. in the earlier part to ±1 m.y. in the later part at the 95% confidence interval for a single analysis (Reilly et al., 2002). Although the previous linear calibrations provide precise estimates of error, they have not been recalibrated to the Gradstein et al. (2004) time scale, except for the younger part of the Miocene where we recalibrated Oslick et al. (1994) to Gradstein et al. (2004) using magnetochronology.

The most comprehensive and robust calibration of $^{87}Sr/^{86}Sr$ variations to age is the look-up table of McArthur et al. (2001, Look-Up Table Version 4) that was recalibrated to Gradstein et al. (2004); we used this and found it provided age estimates that are consistent with biostratigraphic age estimates except for problems in the later middle Miocene. Using a LOWESS (locally weighted scatterplot smoothing) fit,

TABLE 1. STRONTIUM ISOTOPE AGE ESTIMATES

IODP Expedition 313 Site M27					IODP Expedition 313 Site M28					IODP Expedition 313 Site M29				
Sample depth (mcd)	Sr value	error	McArthur et al. (2001) Age (Ma)	Oslick et al. (1994) Age (Ma)	Sample depth (mcd)	Sr value	error	McArthur et al. (2001) Age (Ma)	Oslick et al. (1994) Age (Ma)	Sample depth (mcd)	Sr value	error	McArthur et al. (2001) Age (Ma)	Oslick et al. (1994) Age (Ma)
208.9	0.708832	0.000008	12.0	13.4	226.71	0.708878	0.000027	10.1	12.1	292.28	0.708805	0.000004	13.2	14.2
209.41	0.708819	0.000006	12.6	12.6	231.25	0.708816	0.000026	12.7	13.9	292.28	0.708860	0.000006	10.7	12.6
210.76	0.709010	0.000023	5.6		232.49	0.708745	0.000028	15.5		295.49	0.708814	0.000005	12.8	14.0
213.15	0.708821	0.000005	12.5	12.5	234.40	0.708785	0.000009	14.8	14.8	295.49	0.708854	0.000006	10.9	12.8
223.41	0.708796	0.000007	14.3	14.5	235.93	0.708839	0.000009	11.5	13.2	298.66	0.708861	0.000006	10.6	12.6
229.44	0.708750	0.000008	15.1		237.43	0.708727	0.000035	15.8		300.17	0.708813	0.000006	12.8	14.0
229.44	0.708763	0.000004	15.3		238.83	0.708814	0.000004	12.8	14.0	307.86	0.708914	0.000005	8.9	11.0
243.99	0.708756	0.000007	15.4		243.46	0.708802	0.000009	13.4	14.3	320.31	0.708867	0.000013	10.4	12.4
255.90	0.708727	0.000006	15.8		244.73	0.708817	0.000006	12.7	13.9	322.20	0.708829	0.000006	12.1	13.5
262.04	0.708685	0.000006	16.5		245.04	0.708857	0.000011	10.8	12.7	326.66	0.708834	0.000007	11.9	13.4
262.04	0.708452	0.000005	19.7		245.24	0.708831	0.000011	12.0	13.5	331.84	0.708857	0.000011	10.8	12.7
272.50	0.708665	0.000005	16.9		245.34	0.708818	0.000006	12.6	13.8	333.41	0.708838	0.000006	11.6	13.3
286.76	0.708626	0.000008	17.5		245.44	0.708713	0.000010	16.0		340.27	0.708815	0.000010	12.8	13.9
292.75	0.708625	0.000006	17.5		245.54	0.708808	0.000007	13.1	14.1	352.60	0.708778	0.000006	15.0	
292.75	0.708666	0.000008	16.8		245.84	0.708809	0.000006	13.0	14.1	360.89	0.708831	0.000006	12.0	13.5
305.04	0.708588	0.000006	18.0		245.95	0.708835	0.000005	11.8	13.3	362.50	0.708828	0.000005	12.2	13.6
305.04	0.708640	0.000005	17.3		246.03	0.708826	0.000004	12.3	13.6	371.83	0.708794	0.000004	14.4	14.6
332.15	0.708598	0.000013	17.8		246.04	0.708826	0.000006	12.3	13.6	371.83	0.708801	0.000007	13.5	14.4
332.23	0.708619	0.000011	17.6		246.14	0.708797	0.000008	13.9	14.5	374.31	0.708783	0.000006	14.8	14.9
425.7	0.708466	0.000004	19.5		246.34	0.708848	0.000006	11.1	13.0	411.20	0.708794	0.000006	14.4	14.6
426.71	0.708447	0.000008	19.8		246.44	0.708824	0.000009	12.4	13.7	429.83	0.708721	0.000007	15.9	
431.26	0.708413	0.000004	20.4		246.54	0.708796	0.000005	14.3	14.5	435.74	0.708754	0.000006	15.4	
431.26	0.708416	0.000007	20.3		246.64	0.708830	0.000013	12.1	13.5	439.85	0.708753	0.000004	15.4	
441.08	0.708459	0.000005	19.6		246.74	0.708858	0.000006	10.7	12.7	451.25	0.708787	0.000005	14.7	14.8
441.08	0.708441	0.000015	19.9		246.84	0.708835	0.000006	11.8	13.3	453.74	0.708798	0.000006	13.8	14.4
443.76	0.708399	0.000015	20.6		250.73	0.708810	0.000005	13.0	14.1	455.99	0.708789	0.000004	14.6	14.7
445.26	0.708418	0.000008	20.3		253.06	0.708808	0.000006	13.1	14.1	460.50	0.708824	0.000006	12.4	13.7
454.48	0.708464	0.000006	19.6		253.89	0.708761	0.000014	15.3		463.27	0.708771	0.000006	15.1	
462.07	0.708441	0.000022	19.9		253.94	0.708805	0.000006	13.2	14.2	469.14	0.708748	0.000005	15.5	
463.61	0.708401	0.000006	20.6		253.97	0.708798	0.000006	13.8	14.4	484.42	0.708791	0.000007	14.6	14.7
464.605	0.708402	0.000006	20.6		254.18	0.708002	0.000007	29.3		490.52	0.708785	0.000004	14.8	14.8
468.08	0.708412	0.000006	20.4		260.28	0.708771	0.000005	15.1		514.88	0.708771	0.000007	15.1	
469.79	0.708433	0.000006	20.0		260.36	0.708806	0.000009	14.6	14.2	521.19	0.708761	0.000005	15.3	
475.81	0.708484	0.000008	19.3		263.13	0.708790	0.000005	15.0	14.7	528.20	0.708738	0.000005	15.6	
480.53	0.708426	0.000008	20.1		263.35	0.708807	0.000008	14.5	14.2	528.20	0.708757	0.000004	15.4	
482.54	0.708398	0.000005	20.6		264.83	0.708817	0.000006	14.2	13.9	533.70	0.708745	0.000006	15.5	
482.54	0.708412	0.000006	20.4		265.58	0.708767	0.000006	15.2		545.39	0.708743	0.000006	15.6	
487.68	0.708386	0.000009	20.9		266.13	0.708792	0.000008	15.0	14.6	545.39	0.708745	0.000005	15.5	
489.65	0.708835	0.000008	11.8		266.13	0.708810	0.000006	14.4	14.1	551.55	0.708729	0.000006	15.8	
490.79	0.708431	0.000016	20.0		266.28	0.708814	0.000008	14.3	14.0	557.73	0.708703	0.000006	16.2	
495.36	0.708510	0.000006	19.0		266.38	0.708831	0.000008	13.8	13.5	563.86	0.708744	0.000006	15.5	
495.46	0.708397	0.000005	20.7		266.48	0.708870	0.000013	12.7	12.3	569.80	0.708733	0.000008	15.7	
495.55	0.708439	0.000019	19.9		266.58	0.708789	0.000005	15.1	14.7	573.21	0.708757	0.000008	15.4	
495.87	0.708397	0.000003	20.7		266.66	0.708793	0.000004	14.9	14.6	576.02	0.708745	0.000006	15.5	
518.5	0.708187	0.000006	24.2		266.78	0.708789	0.000006	15.1	14.7	577.645	0.708723	0.000013	15.9	
538.295	0.708036	0.000006	28.6		268.83	0.708802	0.000006	14.7	14.3	588.20	0.708706	0.000004	16.1	
542.48	0.708054	0.000006	28.1		268.93	0.708800	0.000006	14.7	14.4	620.52	0.708643	0.000013	17.2	

(*continued*)

TABLE 1. STRONTIUM ISOTOPE AGE ESTIMATES (*continued*)

IODP Expedition 313 Site M27					IODP Expedition 313 Site M28					IODP Expedition 313 Site M29				
Sample depth (mcd)	Sr value	error	McArthur et al. (2001) Age (Ma)	Oslick et al. (1994) Age (Ma)	Sample depth (mcd)	Sr value	error	McArthur et al. (2001) Age (Ma)	Oslick et al. (1994) Age (Ma)	Sample depth (mcd)	Sr value	error	McArthur et al. (2001) Age (Ma)	Oslick et al. (1994) Age (Ma)
550.25	0.708031	0.000007	28.6		268.93	0.708783	0.000017	15.2	14.9	621.67	0.708688	0.000006	16.4	
560.94	0.708014	0.000006	29.0		269.15	0.708829	0.000007	13.9	13.5	641.08	0.708630	0.000008	17.4	
564.21	0.708023	0.000006	28.8		287.98	0.708847	0.000006	13.3	13.0	650.56	0.708617	0.000007	17.6	
567.38	0.708073	0.000005	27.5		291.62	0.708785	0.000009	14.8		669.17	0.708609	0.000008	17.7	
570.23	0.708030	0.000006	28.6		292.00	0.708764	0.000006	15.2		675.22	0.708350	0.000014	21.5	
570.555	0.708137	0.000013	25.5		293.40	0.708790	0.000006	14.6	14.7	695.29	0.707986	0.000008	29.7	
576.16	0.708053	0.000006	28.1		296.58	0.708763	0.000006	15.3		695.29	0.708596	0.000004	17.9	
579.20	0.708027	0.000004	28.7		297.53	0.708759	0.000006	15.3		747.27	0.708406	0.000005	20.5	
585.10	0.708026	0.000004	28.7		298.14	0.708786	0.000009	14.8	14.8	752.86	0.708386	0.000005	20.9	
591.32	0.708011	0.000004	29.1		299.03	0.708772	0.000006	15.1		753.565	0.708429	0.000009	20.1	
594.36	0.707974	0.000007	30.1		299.48	0.708783	0.000005	14.8	14.9					
619.00	0.708011	0.000004	29.1		299.65	0.708739	0.000006	15.6						
628.09	0.707816	0.000005	33.7		299.72	0.708746	0.000005	15.5						
					301.25	0.708788	0.000007	14.7	14.7					
					302.62	0.708760	0.000008	15.3						
					305.76	0.708771	0.000007	15.2						
					307.32	0.708807	0.000021	13.1						
					310.98	0.708737	0.000008	15.7						
					311.43	0.708802	0.000005	13.4						
					312.12	0.708777	0.000009	15.1						
					312.40	0.708759	0.000008	15.3						
					312.42	0.708775	0.000004	15.1						
					312.42	0.708768	0.000006	15.2						
					312.52	0.708753	0.000006	15.4						
					312.82	0.708773	0.000006	15.1						
					312.82	0.708774	0.000006	15.2						
					312.92	0.708820	0.000006	13.8						
					313.32	0.708766	0.000007	15.2						
					320.02	0.708752	0.000004	15.4						
					320.12	0.708755	0.000007	15.4						
					320.12	0.708791	0.000013	14.7						
					320.52	0.708749	0.000004	15.5						
					320.62	0.708809	0.000006	14.1						
					320.70	0.708786	0.000008	14.8						
					320.80	0.708747	0.000006	15.5						
					321.10	0.708782	0.000005	14.9						
					321.20	0.708747	0.000006	15.5						
					321.50	0.708791	0.000008	14.7						
					322.50	0.708774	0.000008	15.2						
					323.67	0.708725	0.000004	15.8						
					323.92	0.708699	0.000006	16.3						
					324.06	0.708767	0.000006	15.2						
					324.10	0.708758	0.000005	15.3						
					325.40	0.708720	0.000006	15.9						
					333.18	0.708737	0.000006	15.7						
					333.22	0.708778	0.000006	15.0						
					342.76	0.708724	0.000006	15.9						

(*continued*)

TABLE 1. STRONTIUM ISOTOPE AGE ESTIMATES (*continued*)

IODP Expedition 313 Site M27					IODP Expedition 313 Site M28					IODP Expedition 313 Site M29				
Sample depth (mcd)	Sr value	error	McArthur et al. (2001) Age (Ma)	Oslick et al. (1994) Age (Ma)	Sample depth (mcd)	Sr value	error	McArthur et al. (2001) Age (Ma)	Oslick et al. (1994) Age (Ma)	Sample depth (mcd)	Sr value	error	McArthur et al. (2001) Age (Ma)	Oslick et al. (1994) Age (Ma)
					352.95	0.708706	0.000004	16.1						
					358.33	0.708719	0.000005	15.9						
					359.86	0.708689	0.000005	16.4						
					361.02	0.708691	0.000006	16.4						
					364.12	0.708661	0.000006	16.9						
					366.94	0.708678	0.000006	16.6						
					379.42	0.708679	0.000006	16.6						
					385.47	0.708682	0.000006	16.6						
					386.97	0.708673	0.000007	16.7						
					388.49	0.708675	0.000006	16.7						
					389.34	0.709130	0.000014							
					391.26	0.708634	0.000005	17.4						
					402.39	0.708622	0.000006	17.5						
					408.00	0.708637	0.000006	17.3						
					414.30	0.708634	0.000005	17.4						
					418.09	0.708644	0.000008	17.2						
					420.26	0.708669	0.000006	16.8						
					425.12	0.708661	0.000005	16.9						
					432.02	0.708603	0.000006	17.8						
					433.04	0.708620	0.000006	17.6						
					438.39	0.708627	0.000007	17.5						
					447.75	0.708624	0.000007	17.5						
					452.32	0.708611	0.000007	17.7						
					453.54	0.708598	0.000006	17.8						
					461.38	0.708620	0.000006	17.6						
					464.10	0.708610	0.000006	17.7						
					476.12	0.708610	0.000006	17.7						
					478.32	0.708590	0.000007	17.9						
					482.35	0.708625	0.000009	17.5						
					482.53	0.708559	0.000011	18.3						
					482.82	0.708638	0.000009	17.3						
					484.12	0.708610	0.000008	17.7						
					485.43	0.708580	0.000016	18.1						
					487.68	0.708596	0.000004	17.9						
					494.82	0.708621	0.000006	17.6						
					500.26	0.708611	0.000006	17.7						
					501.84	0.708621	0.000005	17.6						
					503.79	0.708574	0.000004	18.1						
					505.62	0.708623	0.000006	17.5						
					507.29	0.708634	0.000004	17.4						
					507.89	0.708644	0.000005	17.2						
					512.17	0.708613	0.000006	17.7						
					668.63	0.708427	0.000004	20.1						

Note: Blank spaces indicate that no age estimate was made using that model. IODP—Integrated Ocean Drilling Program; mcd—meters composite depth.

McArthur et al. (2001) derived typical errors to the fit of ±0.055–0.1 m.y. for the Oligocene to middle Miocene; however, these error estimates do not include errors in the rate of change of Sr through time and external precision (sample reproducibility). We computed the errors in the McArthur et al. (2001) LOWESS fit by determining the rate of change of Sr and dividing into an error estimate of 0.000008 (external precision) plus the difference between the upper and lower Sr isotopic estimates for a given level (interpolated to 0.05 m.y. intervals). The results (Fig. 3, errors for Sr isotope age estimates) are similar to but slightly less than that given from linear regression analysis: resolution is poor in sediments younger than 15 Ma (~±0.75 to ±1.5 m.y.), is excellent from ca. 15 to 25 Ma (~±0.25 to ±0.5 m.y.), and good from ca. 25 to 34 Ma (~±0.5 to ±1.0 m.y.).

Biostratigraphy

Samples examined for calcareous nannofossils were prepared using standard smear-slide techniques (e.g., Bown and Young, 1998). A small amount of sediment was scraped onto a coverslip, mixed with a drop of water, and spread evenly. The coverslip was then dried on a hotplate, affixed to a glass microscope slide using Norland Optical Adhesive 61, and cured under an ultraviolet light. Preliminary age assignments were made through qualitative assessment every ~10 m on an Olympus BX51 light microscope using cross-polarized and plane-transmitted light, with additional samples taken to refine the position of biostratigraphic events. This assessment recorded the average number of each species observed within a field of view (or multiple fields of view) at 1000×, which was then given a qualitative abundance assignment (e.g., rare, few, common). Additional fields of view were scanned at lower magnification (typically 630×) for rare taxa (Tables T4, T4, and T3 *in* Expedition 313 Scientists 2010a, 2010b, and 2010c, respectively). To refine the preliminary age assessments, semiquantitative analysis of assemblages was conducted on a Zeiss Axiophot light microscope by counting 500 specimens in random fields of view at 1000×, followed by scanning additional fields of view at lower magnification to search for rare taxa (Kulhanek, personal data). For samples with lower overall abundances of calcareous nannofossils, the total number of specimens observed in 800 fields of view was counted.

Taxonomic concepts for species are those given in Perch-Nielsen (1985) and Bown (1998). The calcareous nannofossil assemblages are tied to the zonation scheme of Martini (1971). This zonation is commonly used as a basis for worldwide correlation, even though some of the original zonal markers have been shown to be unreliable. Some have suggested alternate or additional markers for some horizons (see discussions in Perch-Nielsen, 1985; Bown, 1998); however, there has been no comprehensive revision of this zonation scheme since its original publication. In addition to tying the nannofossil assemblages to this standard zonation scheme, the age estimates of biostratigraphic events were also used for the chronostratigraphic framework. Age estimates for bioevents from the qualitative data were taken primarily from Berggren et al. (1995) and a few additional sources (see Table T1 in Expedition 313 Scientists, 2010d) and tied to the geomagnetic polarity time scale of Cande and Kent (1995) (Fig. F12 in Expedition 313 Scientists, 2010d). Age estimates for bioevents from the semiquantitative data are those compiled in Gradstein et al. (2004).

Diatoms were generally common to abundant and moderately to well preserved in the Expedition 313 Miocene section. The sequences at Site M29 were studied in much more detail for diatom biostratigraphy than the sequences at Sites M27 and M28 because it was finer grained and had better diatom preservation. Samples were assigned to zones using the East Coast Diatom Zone (ECDZ) biostratigraphy of Andrews (1988) (updated in Barron, 2003). The refined zonal scheme incorporates datum levels developed at Pacific Ocean sites relies upon planktonic diatoms (Barron, 2003), whereas the Andrews (1988) zonation relied upon benthic diatoms. Assignment to diatom zones is given in Tables 1, S1, and S2z of Barron et al. (2013). The diatom zones were calibrated to the Gradstein et al. (2004) time scale (by one of us; Barron et al., 2013).

Dinocysts were processed using standard techniques using HCl and concentrated HF and samples mounted on glass slides using glycerine jelly (McCarthy et al., 2013). Palynomorphs were counted at 400× magnification, with specimens examined under oil immersion at 1000× for verification where necessary (McCarthy et al., 2013). The dinocyst data (Tables 1 and 2 *in* McCarthy et al., 2013) are presented semiquantitatively as relative abundances (rare: <5%; common: 5%–20%, abundant: >20%) based on minimum counts of 30 cysts, although counts normally exceed 60 cysts except at most sequence boundaries and in sparse, terrigenous Serravallian sediments. Zones were assigned to samples using the DN zones of de Verteuil and Norris (1996) (Fig. 2) calibrated to the Gradstein et al. (2004) time scale. In addition, more recent dinocyst studies, most notably the North Sea zonations of Dybkjaer and Piasecki (2008, 2010), were also useful assigning age estimates and in characterizing sequences according to their palynological content. Useful datum levels (calibrated to the Gradstein et al., 2004 time scale) in Holes 27A and 29A are listed in Tables 1 and 2 of McCarthy et al. (2013).

The onshore science party (Mountain et al., 2010) reported age estimates to the Berggren et al. (1995) time scale. All figures and age estimates reported here are calibrated to the Gradstein et al. (2004) time scale and its updates (Fig. 4, time scale used), which differ from the Berggren et al. (1995) time scale by the placement of the Oligocene-Miocene boundary at 23.0 Ma versus 23.8 Ma. This shifts the early Miocene magnetochrons and biozones (the target of Expedition 313) to slightly younger ages because the time scales are essentially similar younger than 16 Ma. The Gradstein et al. (2004) time scale and the Gradstein et al. (2012) time scales are essentially the same in this interval except that the Langhian-Burdigalian boundary is 0.17 m.y. older in the Gradstein et al. (2012) time scale.

Resolution

Age resolution in Expedition 313 sediments depends upon the preservation of fossils and carbonate for Sr isotopic measurements

Figure 4 (*on following page*). Age-depth plot for Integrated Ocean Drilling Program Expedition 313 Site M27. Axes are depth in meters composite depth (mcd) and age in millions of years (Ma); time scale of Gradstein et al. (2004); diatom zone calibration to the Gradstein et al. (2004) time scale is after Barron (2003); dinocyst calibration is after McCarthy et al. (2013). Downhole gamma log is show in counts per second (cps). Cumulative percent lithology data are after Miller et al. (2013b). Sequence boundaries are indicated with red horizontal lines; precise depths are indicated (in mcd) and age estimates are in red (Ma). Sr isotope data are shown as solid dots, with conservative errors of ±0.6 m.y. for samples older than 15 Ma and ±1.17 for samples younger than 15 Ma (Oslick et al., 1994). Biostratigraphic errors are for zones and subzones as indicated in text (dinocysts—green; nannofossils—blue; diatoms—purple). Core recovery on far right column shows core numbers and recovered intervals in black. Lines of accumulation (sedimentation rates) are in black (see text); scale on right illustrates various sedimentation rates. Priab.—Priabonian.

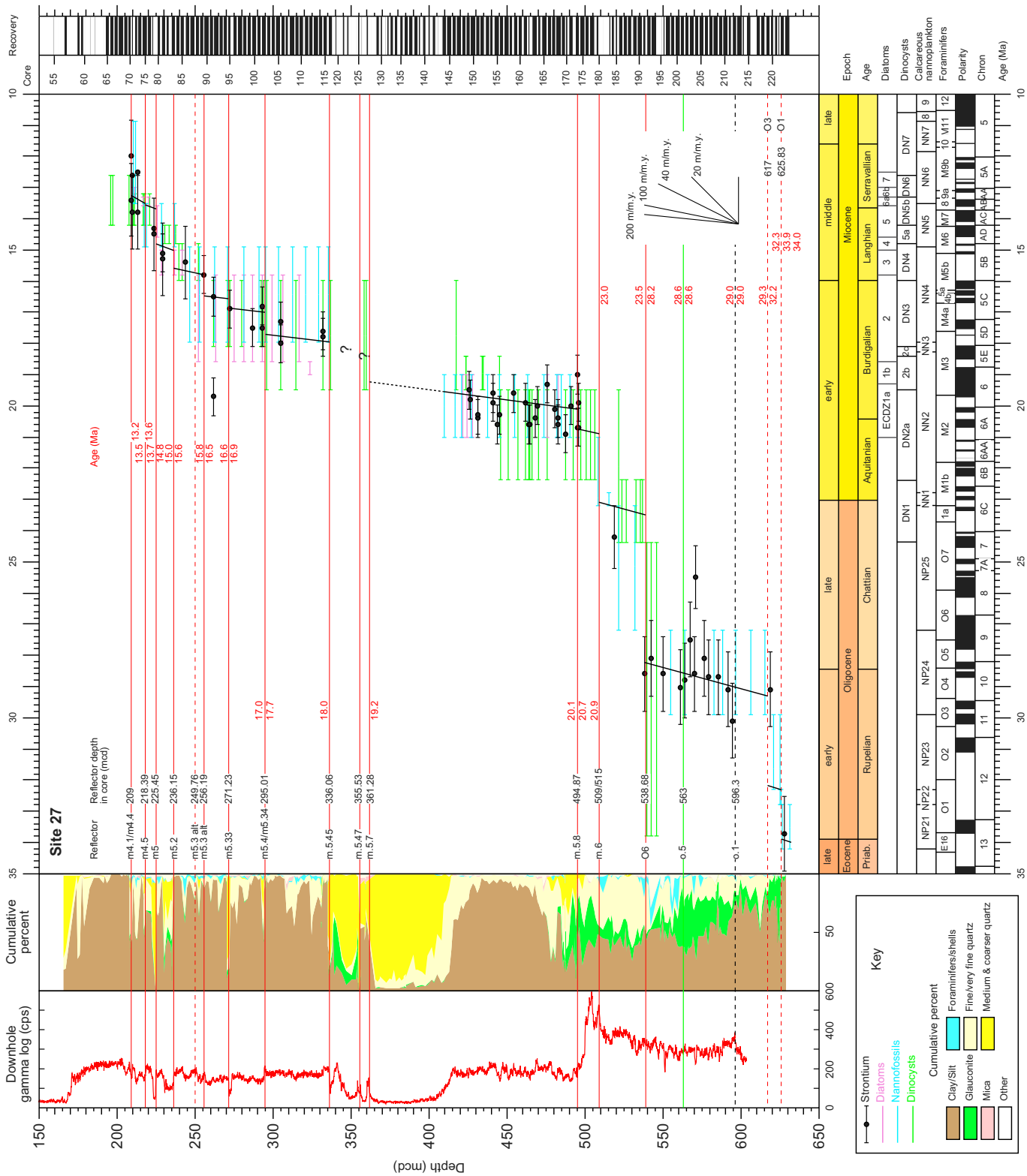
Site 27
Reflector
Reflector depth in core (mcd)
Age (Ma)
Recovery
Core
Cumulative percent
Downhole gamma log (cps)
Depth (mcd)
Epoch
Age
Diatoms
Dinocysts
Calcareous nannoplankton
Foraminifers
Polarity
Chron
Age (Ma)
Eocene
Oligocene
Miocene
Priab.
Rupelian
Chattian
Aquitanian
Burdigalian
Langhian
Serravallian
early
late
middle
200 m/m.y.
100 m/m.y.
40 m/m.y.
20 m/m.y.
Key
Strontium
Diatoms
Nannofossils
Dinocysts
Cumulative percent
Clay/Silt
Foraminifers/shells
Glauconite
Fine/very fine quartz
Mica
Medium & coarser quartz
Other

Figure 4.

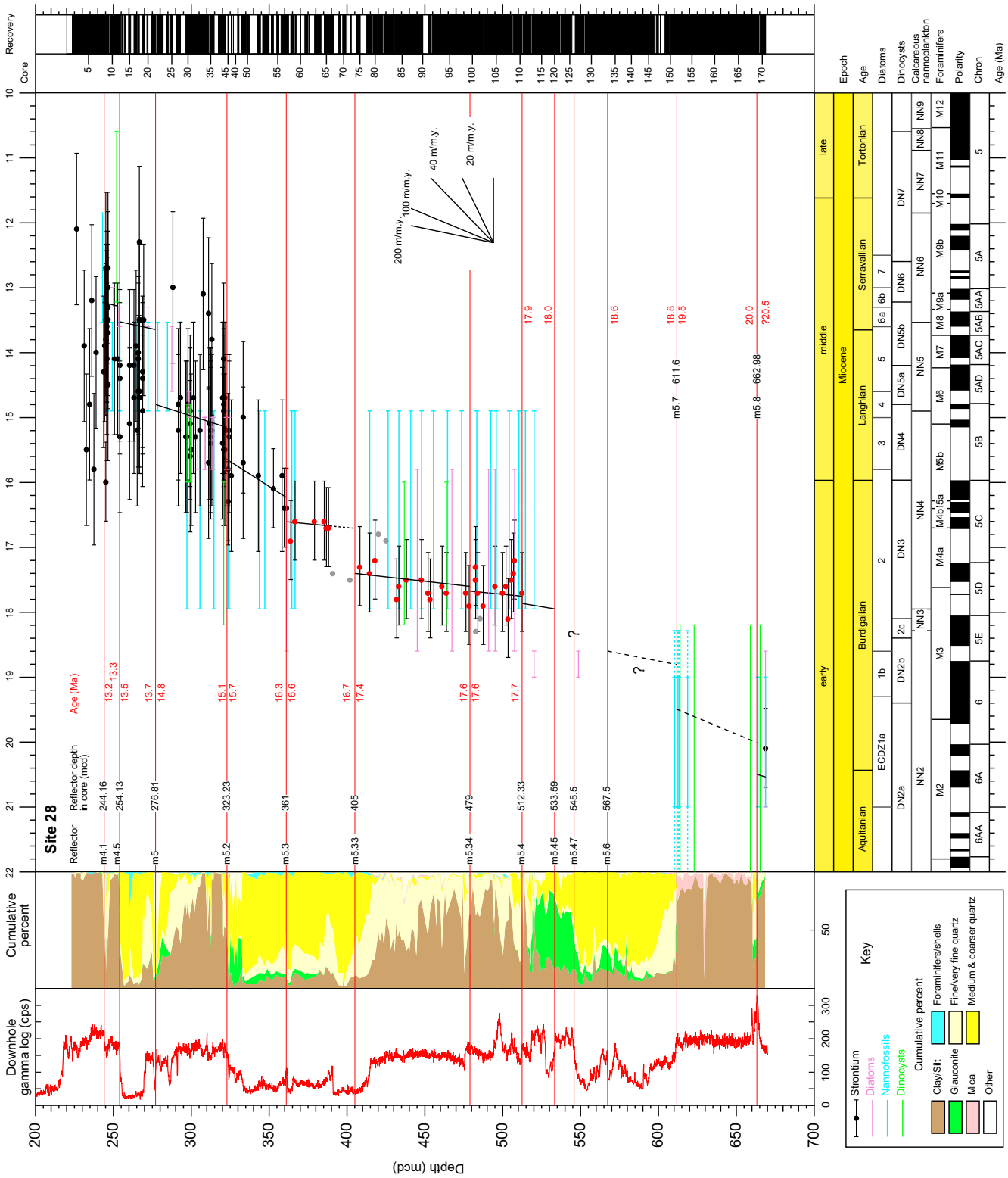

Figure 5. Age-depth plot for Integrated Ocean Drilling Program Expedition 313 Site M28. Aquitan.—Aquitanian. Caption as in Figure 4.

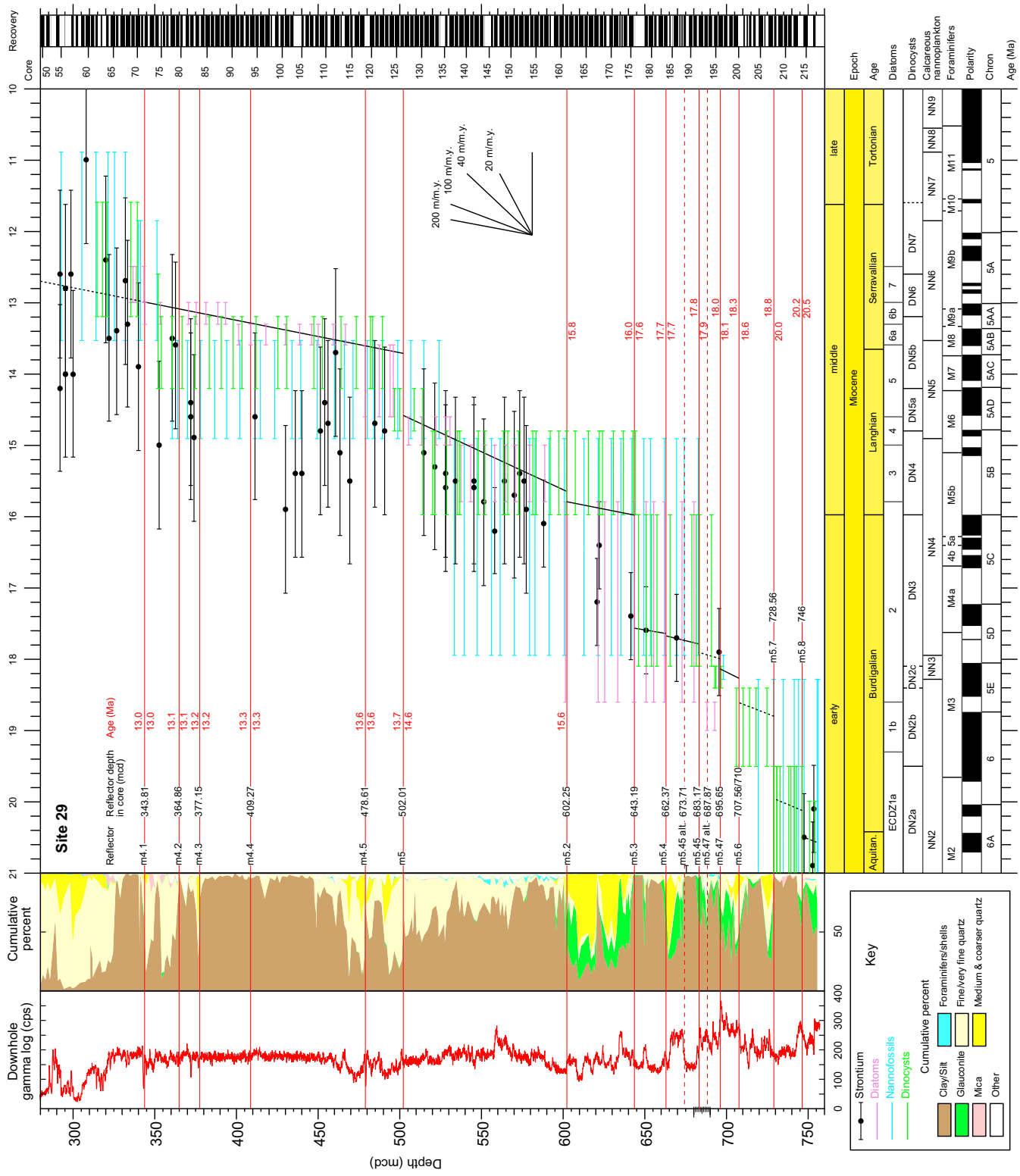

Figure 6. Age-depth plot for Integrated Ocean Drilling Program Expedition 313 Site M29. Aquitan.—Aquitanian. Caption as in Figure 4.

(typically 4–6 mg). Sufficient carbonate for Sr isotopic study was found in 14 of 18 Eocene–Miocene sequences at Site M27, 10 of 14 sequences at M28, and 13 of 15 sequences at Site M29 (Figs. 4–6). Sr age estimates are complicated by low age resolution in sediments younger than 15 Ma (e.g., sequences m5.2 to m4.1; Figs. 4–6), reworking of sediments (especially above sequence boundary m5; Figs. 2 and 4–6), and rare diagenetic alteration indicated by several discordant age estimates. In optimum conditions there are abundant, well-preserved, in situ shells and foraminiferal tests for Sr analysis that can be integrated with nannofossil, diatom, and dinocyst zonations. Some sequences were sampled in their thickest part, and biostratigraphy using several groups and Sr isotopes could be combined. Commonly there is a crossover from one biozone to another within these thick sequences, allowing datum levels to place firm constraints on age estimates. By integrating the various dating tools, Expedition 313 sediments can be dated to within a fraction of a biozone. Resolution of ~±0.25–0.5 m.y. is attainable in these sequences (see Discussion). Many sequences could only be correlated to one long-ranging biozone and had few shells for dating and have relatively large errors; for these sequences age resolution is the length of the zone, typically ±1 m.y.

Sequence Interpretation

Expedition 313 cored and logged 19 sequences in the three boreholes: 1 Eocene, 3 Oligocene, and 15 Miocene sequences. Sequence boundaries were recognized in Expedition 313 cores in two ways (Miller et al., 2013b). First, sequence boundaries were identified on seismic profiles using criteria of onlap, downlap, toplap, and erosional truncation (Monteverde et al., 2008; Monteverde, 2008). By establishing a velocity function for the sediments, predicted depths to the surfaces encountered on the seismic profiles were calculated (Mountain et al., 2010). On Expedition 313, sequence boundaries were also interpreted from the cores using the physical stratigraphy preserved in the cores, downhole and core log data, and by using abrupt facies changes across surfaces in the cores that showed evidence of erosion and/or hiatuses (Mountain et al., 2010; Miller et al., 2013b). The two methods were then compared and discrepancies were resolved to best place each sequence boundary (Mountain et al., 2010). Updated placement of sequence boundaries based on integration of seismic profiles, core and log evidence, and synthetic seismograms and an updated velocity-depth function of Mountain and Monteverde (2012) are provided in Miller et al. (2013b). We tabulate depths of the sequence boundaries (Table 2) (from Miller et al., 2013b) and use them on the age-depth diagrams that compare Sr isotopic and biostratigraphic data with surfaces and sedimentological and log evidence (Figs. 4–6). Eocene and Oligocene sequences were not imaged well on seismic profiles and only sampled at Site M27 (Fig. 5). Placement of Eocene to Oligocene sequence boundaries are based on hiatuses determined using Sr isotopes and biostratigraphy, core surfaces, and facies successions observed in cores (Mountain et al., 2010; Miller et al., 2013b; Fig. 4).

A detailed discussion of the criteria and rationale for placing sequence boundaries was presented in Mountain et al. (2010) and is updated in Miller et al. (2013b). Detailed observations of Miocene facies changes and systems tracts within sequences were presented in Mountain et al. (2010) and in Miller et al. (2013c). We include gamma logs on the age-depth plots because gamma-log increases and peaks are associated with most of the sequences boundaries (e.g., 11 of 14 at Site M28, Fig. 4; 12 of 13 at Site M28, Fig. 5; 5 of 13 at Site M29, Fig. 6), helping to illustrate their placement. Similarly, we include cumulative percent data that help elucidate the sequence boundaries and trends within sequences. Cumulative lithology was determined by quantitatively measuring weight percent very fine sand, medium sand and coarser sediment, and silt-clay on washed samples and semiquantitatively estimating the percent glauconite, shells, and mica through visual counts (data provided in Miller et al., 2013b). Percent sand-sized carbonate material is shown (blue in Figs. 4–6), indicating particularly shell-rich intervals most suitable for Sr isotopic stratigraphy. These two datasets and the placement of the sequence boundaries are discussed in detail in Miller et al. (2013b); they are shown here as a means of integrating our age control with these studies. We include a table (Table 1) of depths and age estimates of sequence boundaries here (see also Table 1 *in* Miller et al., 2013b).

RESULTS

Eocene Sequence

The oldest sequence found by Expedition 313 drilling was below an unnamed core surface (625.83 meters composite depth, mcd) tentatively identified as a sequence boundary at Site M27 (Fig. 4). This sequence boundary has no seismic expression and the bottom of the sequence was not cored. It is assigned to calcareous nannoplankton Zone NP21 and has an Sr isotopic age estimate of 33.7 Ma. Zone NP21 (34.2–32.8 Ma) straddles the Eocene-Oligocene boundary (33.9 Ma). One specimen of *Tuborotalia* cf. *pomeroli* suggests correlation to the Eocene, and we tentatively assign an age of 34.0–33.9 Ma to this sequence.

Oligocene Sequences

Three sequences were resolved in the Oligocene section at Site M27 (Fig. 4). These sequences are not imaged on the seismic data, but are identified by core and log observations. Oligocene sequences have minimal lithologic and seismic expression due to deep-water locations on clinoform bottomsets. The oldest Oligocene sequence is between the possible sequence boundary at 625.83 mcd and a faint surface that is interpreted as a sequence boundary at 617 mcd. Calcareous nannoplankton at the base of the sequence (625.7 and 625.0 mcd) are assigned to early Oligocene Zone NP22, whereas samples at 624.7 and 620.8 mcd are assigned to Zone NP23. A Sr isotope age estimate at 619.0 mcd (29.1 Ma, biochron NP24) is interpreted as burrowed down because it yields the same age as the sequence above. It is possible that that there are two very thin sequences (one in NP22 and one in NP23), but there is no evidence in the cores for a sequence boundary and we prefer to interpret the sediments as having been deposited across the NP22-NP23 boundary. It is also possible that *Reticulofenestra umbilicus* (the last occurrence of which marks the base of Zone NP23) and *Isthmolithus recurvus* (which has a last occurrence in upper Zone NP23) are reworked and the sequence in entirely within Zone NP23. However, we favor assignment to Zone NP22 and lower NP23 and interpret an age of ca. 32.3–32.2 Ma. This sequence appears to correlate with onshore New Jersey sequence O1 that straddles the NP22-23 boundary, and we adopt that term here.

A thick (~78 m) Oligocene sequence is found between sequence boundaries at 617 mcd and a heavily bioturbated contact at 538.68 mcd that is interpreted as a sequence boundary (Fig. 4). The lower sequence boundary at 617 mcd is not resolved seismically, but is resolved in the cores and interpreted as a sequence boundary based on evidence for a several million year hiatus (Mountain et al., 2010; this study; Fig. 4). Calcareous nannoplankton indicate that the sequence from 617 to 538.68 mcd was deposited in Zone NP24 (29.9–27.2 Ma); 12 Sr isotopic age estimates were obtained from this sequence. In addition, a sample at 619 mcd, just below the lower contact, and one at 538.3 mcd, just above the upper contact, gave age estimates that were identical to the age estimates obtained in this sequence; they are assumed to be burrowed down (619 mcd) or reworked (538.3 mcd) from

TABLE 2. EXPEDITION 313 SEQUENCE DEPTH AND AGES

IOPD Site M27			IOPDSiteM28			IOPDSiteM29		
Sequence	Depth (mcd)	Age (Ma)	Sequence	Depth (mcd)	Age (Ma)	Sequence	Depth (mcd)	Age (Ma)
	0	0.72						
uP3	13.57	0.85						
	13.57	0.19						
uP1	21.42/22.8	0.22						
	21.42/22.8	1.03?						
*lP2	26.4	1.08?						
	26.4	1.4?						
*lP1	31.9	1.5?						
	31.9							
m1	96	NR						
	96							
m3	111	NR						
	111							
m4	135	NR						
	135							?12.6
m4.1	209		m4.1	244.16	?	m4.1	342.81	13
							342.81	13
						m4.2	364.86	13.1
							364.86	13.1
						m4.3	377.15	13.2
							377.15	13.2
						m4.4	408.65	13.3
	209	13.2		244.16	13.2		408.65	13.3
m4.5	218.39	13.5	m4.5	254.23	13.3	m4.5	478.61	13.6
	218.39	13.6		254.23	13.5		478.61	13.6
m5	225.45	13.7	m5	276.81	13.7	m5	502.01	13.7
	225.45	14.8		276.81	14.8		502.01	14.6
m5.2	236.15	15	m5.2	323.23	15.1	m5.2	602.25	15.6
	236.15	15.6		323.23	15.7		602.25	15.8
m5.3alt.	249.76							
m5.3	256.19	15.8	m5.3	361.0	16.3	m5.3	643.19	16.0

(*continued*)

this sequence, and they were included in the age analysis. Most of the age estimates cluster between 30.1 Ma (594.36 mcd) and 28.1 Ma (542.28 mcd). A discordant Sr isotopic age estimate of 25.5 Ma (570.56 mcd) is assumed to have been altered. Linear regression through the points gives an age of 28.2 Ma for the upper surface and an age of 29.3 Ma for the lower surface. This sequence has a sedimentation rate of ~100 m/m.y. (Fig. 4) and correlates with onshore New Jersey sequence O3 of Pekar et al. (2001); we adopt this name here.

Two poorly resolved Oligocene seismic surfaces have been traced into Site M27. Reflector o.5 ties approximately to 563 mcd (Mountain et al., 2010; Miller et al., 2013b) within sequence O3 (Fig. 4) and has an age of ca. 28.6 Ma. A very poorly resolved reflector (o.1), tentatively placed at 596.3 mcd, has an age of ca. 29 Ma. Considering the uncertainty in the depth of this seismic reflector, it could be equivalent to the 617 mcd basal sequence boundary of sequence O3. Alternatively, reflector o.1 may be associated with a maximum flooding surface (Miller et al., 2013b) because it is best correlated with a major gamma-log peak at 597 mcd and a facies change from clay below to glauconite-quartz sands above.

The youngest Oligocene sequence (538.68–509 to 515 mcd) is not recognized seismically, but it is clearly a sequence because there are >1-m.y.-year hiatuses associated with the bounding surfaces above and below (Fig. 4). It was deposited across calcareous nannoplankton Zone NP25-NN1 boundary (23.1 Ma at ~520 mcd). This is consistent with the dinocyst data

TABLE 2. EXPEDITION 313 SEQUENCE DEPTH AND AGES (*continued*)

IOPD Site M27			IOPDSiteM28			IOPDSiteM29		
Sequence	Depth (mcd)	Age (Ma)	Sequence	Depth (mcd)	Age (Ma)	Sequence	Depth (mcd)	Age (Ma)
	256.19	16.5		361.0	16.6			
m5.33	271.23	16.6	m5.33	405.0	16.7			
				405.0	17.4			
m5.34	cutout		m5.34	479.0	17.6			
				479.0	17.6			
	271.23	16.9					643.19	17.6
m5.4	295.01	17.0	m5.4	512.33	17.7	m5.4	662.37	17.7
	295.01	17.7		512.33	17.9		662.37	17.7
						m5.45	673.71	17.8
m5.45	336.06	18	m5.45	533.59	18.0	5.45alt.	681	
	336.06	?		533.59	?		673.71	17.9
						m5.45alt.	681	
m5.47	355.53	?	m5.47	545.5	?	m5.47	687.87	18.0
						m5.47alt.	695.65	
	X			545.5	?		687.87	18.1
						m5.47alt.	695.65	
m5.6	X		m5.6	567.5	?	m5.6	707.56/710	18.3
	355.53	?		567.5	18.6		707.56/710	18.6
m5.7	361.28	?	m5.7	611.6	18.8	m5.7	728.56	18.8
	361.28	19.2		611.6	19.5		728.56	20.0
m5.8	494.87	20.1	m5.8	662.98	20.0	m5.8	746	20.2
	494.87	20.7						
m6	509/515	20.9						
	509/515	23						
*O6	538.68	23.5						
	538.68	28.2						
*O3	617	29.3						
	617	32.2						
*O1	625.83	32.3						

Note: IOPD—Integrated Ocean Drilling Program; NR—not resolved; mcd—meters composite depth; X—not present; ?— ; alt.— ; cut out—not present.
*Not resolved on seismic profiles.

(Zone DN1) and a single Sr analysis of 24.2 Ma. The basal age of the sequence is not well constrained. Assuming a sedimentation rate that is comparable to the underlying sequence, the basal age is 23.5 Ma. The top of the sequence cannot be younger than the top of NN1 (22.8 Ma) and is interpreted to be 23.0 Ma based on a best fit to the age data (latest Oligocene; Fig. 4). The sedimentation rate for this sequence is assumed to be 100 m/m.y. using a sedimentation rate from the underlying sequence. Sequence O6 is approximately correlative with sequence O6 of Pekar et al. (2001), although it may be younger than O6 onshore.

Miocene Sequences

Biostratigraphic and Sr isotopic control on 15 Miocene sequences allowed us to determine the age relations of the sediments. The sequences are discussed first at the borehole at which they are best dated.

Sequence m6

Sequence m6 is found at all three Expedition 313 sites. Site M27 penetrated the entire sequence, but Sites M28 and M29 both bottomed in sequence m6. At Site M27, the sequence (509 to 515–494.87 mcd) is poorly dated (Fig. 4). Sample 313–27–179–2 at 10 cm is assigned to calcareous nannoplankton Zone NN1 to NN2 based on the presence of *Helicosphaera recta* plus frequent *Triquetrorhabdulus carinatus*; the HO of these two events occurs in the lower part of NN2. The absence of *Dictyococcites bisectus* (last occurrence in lower NN1) also suggests an age of mid-NN1 to lower NN2 for this sample. Dinocysts assign the sequence to Zone DN2a. Four Sr age estimates were obtained from the top of the sequence. The uppermost age estimate (19.0 Ma at 495.36 mcd) is more similar to the overlying sequence, and the shell from which the age estimate was derived is assumed

to have been burrowed down in the core. The other three samples (see Table 1) have age estimates of 20.7, 19.9, and 20.7 Ma (mean is 20.4 Ma), similar to what was found at the other two sites. The top age for the sequence is constrained by superposition to have been older than 20.1 Ma, the age estimate of the base of the overlying sequence m5.8. Assuming a sedimentation rate similar to the sequences below that have similar lithology, the top of the sequence is dated as 20.7 Ma and the base of the sequence is dated as ca. 20.9 Ma.

At Site M29, sequence m6 is found from 756.33 to 746 mcd and is assigned to Zone NN2; 3 Sr age estimates in this interval have an average age of 20.5 Ma. The top of the sequence is placed at 20.5 Ma; the base was not sampled.

At Site M28, sequence m6 (Fig. 5) is found from 668.66 to 662.98 mcd. The sequence is dated using calcareous nannoplankton as mid-Zone NN2, by dinocysts as Zone DN2 (late Aquitanian to Burdigalian), and by diatoms as ECDZ 1. A Sr isotopic age estimate of 20.1 ± 0.6 Ma was obtained at 668.63 mcd. The top of the sequence is placed ca. 20.5 Ma, to be consistent with Site M29.

Sequence m5.8

Sequence m5.8 is 133.59 m thick at Site M27 (494.87–361.28 mcd), where Expedition 313 drilled through the thickest part of the sequence on the foreset (Fig. 2). It is composed of a lowstand systems tract (LST; 494.87–477.52 mcd), a transgressive systems tract (TST; 477.52 to ~450 mcd), and a thick highstand systems tract (HST; ~450–361.28 mcd) (Miller et al., 2013b, 2013c). The sequence contains numerous shells to ~425 mcd and this interval can be well dated by Sr isotopes. We conducted 21 Sr analyses on shells in this sequence ranging in age from 20.9 Ma (487.68 mcd) to 19.3 Ma (475.81 mcd). We excluded a point from the age-depth plot at 489.65 mcd (12.3 Ma) interpreted as altered due to its discordant age. The sample at 425.7 mcd, the highest sample in which carbonate was found, yielded an age of 19.5 Ma. The sample at 475.81 mcd was not included in the regression because its value was more than 2 standard deviations younger than the points within 10 m of it. A linear regression through the Sr isotope age estimates yields a sedimentation rate of 148 m/m.y. and an age of 20.1 Ma for the base of the sequence m5.8. The top of the sequence, dated by extrapolating the sedimentation rate, is 19.2 Ma, although higher rates of deposition of the sands would yield a slightly older age (as old as 19.5 Ma).

Sequence m5.8 at Site M27 contains calcareous nannoplankton from the lower sequence boundary to 409.6 mcd and is barren above 409 mcd to the upper sequence boundary. The calcareous nannoplankton assemblages are assigned to mid–Zone NN2. Dinocysts are assigned to Zone DN2a–DN2b, consistent with the nannoplankton and the Sr isotope data. However, the regression based on Sr isotopes is slightly older (0.4 m.y.) than the assignment to Zone DN2b at 445.14 mcd. Diatoms are assigned to ECDZ 1, which is consistent with the nannoplankton and the dinocysts.

There was insufficient carbonate for Sr isotope analysis in sequence m5.8 at Site M28 (662.98–611.6 mcd) and Site M29 (746–728.56 mcd). The lithology of this sequence at these two sites is a very distinctive tan prodelta clay (Mountain et al., 2010), and is very different from the lithology at Site M27 (Mountain et al., 2010). Miller et al. (2013c) show that the bulk of the section at Sites M28 and M29 is equivalent to the HST of sequence m5.8 at Site M27.

At Site M29, calcareous nannoplankton in sequence m5.8 are assigned to Zone NN2. Dinocysts are assigned to Zone DN2a and no diatoms were found. The only real age constraint is that it must be younger than the sequence below and within Zone DN2a. In agreement with Site M27, the sequence is placed at 20.2–20.0 Ma, although the age errors on this are ~±1 m.y.

At Site M28, calcareous nannoplankton in sequence m5.8 are assigned to mid-Zone NN2. Dinocysts are assigned to Zone DN2 and diatoms are assigned to ECDZ 1b. If this sequence is equivalent to m5.8 at Site M27, then it was probably deposited between 20.0 and 19.5 Ma, although the error bar on age estimates at M28 is ~±1–1.5 m.y.

Sequence m5.7

Sequence m5.7 is poorly dated at all three sites. At Site M29, sequence m5.7 (728.56 to 707.56–707.56 to 710 mcd) is assigned to Zones NN2 and DN2b. The base of Zone DN2b is poorly constrained globally to ca. 20–19.2 Ma (McCarthy et al., 2013). Placing the sequence in the middle of this zone would give it an age of 18.8–18.6 Ma.

At Site M27 (361.28–355.53 mcd) there is no age information for sequence m5.7 other than assignment to Zone DN2b (younger than 19.4 Ma). At Site M28 (611.6–567.5 mcd), calcareous nannoplankton are found in a single sample (610.56 mcd) in this sequence and are assigned to Zone mid-NN2. This sequence is tentatively assigned an age of 18.8–18.6 Ma, similar to that of Site M29.

Sequence m5.6

Sequence m5.6 was cut out at Site M27 and is not dateable at Site M28 (567.5–545.5 mcd). The sequence is finer grained and contains some carbonate at Site M29 (710 to 707.56–687.87 mcd) and is dated there. Calcareous nannoplankton are assigned to Zone NN3 (18.28–17.95 Ma), dinocysts to Zone DN2c, and diatoms to ECDZ 1. A Sr isotope age estimate of 17.9 Ma (695.3 mcd) is consistent with the nannofossils and dinocysts, although diatom assignment to ECDZ 1 is discordant. The age of this sequence is well constrained at Site M29 because the top of Zone DN2 and the base of Zone NN3 are close in age and their overlap in this sequence at Site M29 provides a datum point. The sequence is dated as 18.3–18.1 Ma with a sedimentation rate of ~100 m/m.y.

Sequence m5.47

Sequence m5.47 is very coarse grained and could not be dated at Site M27 (355.53–336.06 mcd), other than Zone DN2–4 (337.04 mcd; 22.4–14.8 Ma), or at Site M28 (545.5–533.59 mcd). At Site M29 (687.87–673.71 mcd; note that the basal sequence boundary of m5.47 at Site M29 can be alternatively placed at 695.65 mcd, but the placement at 687.87 mcd is preferred; Miller et al., 2013c) calcareous nannoplankton are assigned to Zone NN4 (17.95–14.91 Ma), dinocysts are assigned to Zone DN3, and diatoms are assigned to ECDZ 2 (18.6–15.8 Ma). A single Sr age of 21.5 Ma (675.22 mcd) is considered altered because it is ~2.5 m.y. older than indicated by biostratigraphy and contradicted by superposition of other Sr isotope data. The correlation line for this sequence is tentatively placed where biostratigraphic markers overlap. The sequence is dated as 18.0–17.9 Ma with an assumed sedimentation rate of 140 m/m.y.

Sequence m5.45

At Site M28, sequence m5.45 (533.59–512.33 mcd) is constrained in age by a well-dated sequence above. The overlying sequence is placed in Zone NN4 (i.e., younger than 17.9 Ma). Dinocysts can only be broadly assigned to the early Burdigalian. Diatom assignment to ECDZ 1b is inconsistent with the nannofossil correlation and suggests that the diatoms are slightly miscalibrated. This sequence must be older than the sequence above (sequence m5.4, 17.7–17.6 Ma) and we estimate its age as ca. 18.0–17.9 Ma.

At Site M27, sequence m5.45 (336.03–295.01 mcd) is moderately well dated. Calcareous nannoplankton are assigned to Zone NN4, diatoms to ECDZ 1b and ECDZ 2, and dinocysts to Zone DN3. Four Sr isotope age estimates range from 18.0 to 17.3 Ma. A linear fit to the Sr age estimates agrees with the biostratigraphic markers except assignment of the lower part of the sequence to ECDZ 1b.

This assignment does not agree with nannofossils, and suggests a minor miscalibration of the diatom zone. We assign an age based on the better dated section at Site M28 of 18.0–17.7 Ma, with an assumed sedimentation rate of ~140 m/m.y.

At Site M29, sequence m5.45 (673.71–662.37 mcd) is assigned to ECDZ 2 and Zones DN3 and NN4. An alternate placement of the basal m5.45 sequence boundary at 681 mcd is not preferred (Miller et al., 2013c), and is not used here. The sedimentation rate line for this sequence was drawn through the Sr age assuming the sedimentation rate of 140 m/m.y. obtained for the well-dated m5.4 sequence above, yielding an age estimate of 17.8–17.7 Ma.

Sequence m5.4

Composite sequence m5.4 is best dated at Site M28 (512.33–361 mcd), where it was sampled in the foreset and is 151.33 m thick. It is assigned to Zones NN4, ECDZ 2, and DN3. Linear regression of the Sr data gives a correlation line for the sequence of 17.7–17.3 Ma with a sedimentation rate of 373 m/m.y. This correlation line is consistent with the biostratigraphic data other than a broad dinocyst assignment to DN2 or older in the lower part of the section (Fig. 5). Integration of seismic data and stratigraphy (Miller et al., 2013c) suggests that this sequence is broken into three higher order sequences (m5.4-1, m5.34, and m5.33) dated by regressing the Sr isotope data: (1) sequence m5.4-1 (512.33–479 mcd) is ca. 17.7–17.6 Ma; (2) sequence m5.34 (479.0–405.0 mcd) is 17.6–17.4 Ma; and (3) sequence m5.33 (405.0–361.0 mcd) is 16.7–16.6 Ma, with a 0.7 m.y. hiatus associated with the basal unconformity.

At Site M27, sequence m5.4-1 is cut out and sequence 5.34 (295.01–271.23 mcd) is placed in Zones NN4, DN3, and ECDZ 2. Four Sr age estimates were obtained from this sequence. A correlation line placed through these points dates the sequence as 17.0–16.9 Ma. Sequence m5.33 (271.23–256.19 mcd) is also placed in Zones NN4, DN3, and ECDZ 2. Two of three Sr samples (262.04 mcd [19.7 Ma] and 255.9 mcd [15.8 Ma]) are assumed to be altered or reworked due to their discordant ages and are not used for age interpretation. A correlation line placed through 16.5 Ma at 262.04 mcd gives an age estimate for the sequence of 16.6–16.5 Ma.

At Site M29 sequence m5.4 (662.37–643.19 mcd) is placed in Zones DN3, NN4, and ECDZ 2. Its age is obtained by assuming a sedimentation rate of ~140 m/m.y. from the Sr data, yielding an estimate of 17.7–17.6 Ma. This age is near the oldest part of the composite sequence (m5.4-1) as dated at Site M28, but is not well constrained.

Sequence m5.3

At Site M29, sequence m5.3 (643.19–602.25 mcd) is assigned to ECDZ 2 and Zones NN4 and DN4. Only three Sr age estimates were obtained in this sandy sequence. Two (641.08 and 620.52 mcd) are closer to the age of the underlying sequence and are interpreted as being reworked. The third age (16.4 Ma at 621.67 mcd) is compatible with the biostratigraphy within the large error. The best correlation line for the sequence is placed at the overlap between the biostratigraphic indicators with an age of 16.0–15.8 Ma.

At Site M27, sequence m5.3 (256.19–236.15 mcd) is in Zones NN4, DN4, and ECDZ 2 at the base and in ECDZ 3 on top. One Sr age estimate of 15.4 Ma was obtained (243.99 mcd). The age of the sequence is slightly younger at Site M27 (ECDZ 3, younger than 15.8 Ma) than at Site M29 (ECDZ 2, older than 15.8 Ma). We estimate its age at Site M27 as ca. 15.8–15.6 Ma, timing it at the changeover from ECDZ 2 to ECDZ 3. Zone NN5 occurs at the upper sequence boundary, likely reflecting a local highest occurrence of *Helicosphaera ampliaperta* that occurs prior to the last appearance datum of the species.

At Site M28, sequence m5.3 (361–323.23 mcd) is in ECDZ 2 (at 361.07 mcd near the base of the sequence) and Zone NN4. Sr age estimates range from 16.4 (at 361.02 mcd) to 15.2 Ma (at 324.06 Ma). Using linear regression through the Sr points, the age of the sequence is 16.3–15.7 Ma, with a sedimentation rate of 66 m/m.y.

Sequence m5.2

Sequences younger than sequence m5.3 (i.e., sequence m5.2 and those stratigraphically above it) are not as accurately dated using Sr isotopic stratigraphy. Miocene Sr ratios younger than 15 Ma change more slowly than they do in sediments that are older than 15 Ma. As a result Sr values that are younger than 15 Ma have much larger errors than those that are older (Fig. 3). In addition, age estimates given by Sr isotopes are consistently older than the biostratigraphic markers in Exp. 313 sites, perhaps reflecting reworking of older material.

At Site M29, sequence m5.2 (602.25–502.01 mcd) crosses several biostratigraphic boundaries. It is in Zone NN4 at the bottom and Zone NN5 at top. It is ECDZ 3 at the bottom and ECDZ 4 at top. It is in Zone DN4 at the bottom and appears to be in Zone DN5 at top; 15 Sr isotopic age estimates in this sequence range from 16.1 Ma (588.2 mcd) near the base to 15.1 Ma (514.88 mcd) near the top and are too old to be in agreement with the age estimates of the biostratigraphic indicators, which are in very good accord. This sequence illustrates the limits of relying on Sr isotopes for sections younger than 15 Ma. As a result, the correlation line follows the biostratigraphic age assignments, yielding an age estimate of 15.6–14.6 Ma (Fig. 6).

At Site M27, sequence m5.2 (236.15–225.45 mcd) is in ECDZ 3 at the bottom and in ECDZ 4 at the top and it is in Zones NN5 and DN5a. The ECDZ 3-ECDZ 4 boundary (15.0 Ma) is within this sequence m5.2 at all three sites, providing a tie point. Two Sr age estimates of 15.3 and 15.1 Ma (both at 229.44 mcd) are compatible with the biostratigraphy. The biostratigraphy is not completely in agreement, but a correlation line can be placed so that it is close to all the markers. The age of the sequence is 15.0–14.8 Ma.

At Site M28, sequence m5.2 (323.23–276.81 mcd) is in ECDZ 3 at the bottom and ECDZ 4 at top. It also changes from Zone NN4 at bottom to Zone NN5 at top. The Sr age estimates are scattered (ca. 16.2–12.9 Ma) in this sequence, suggesting possible reworking of older material. The correlation line is fit through the biostratigraphic data and yields a sedimentation rate of ~150 m/m.y. The age estimate for the sequence is 15.1–14.8 Ma (Fig. 5).

Sequence m5

At Site M27, sequence m5 (225.45–218.39 mcd) is in ECDZ 6a and Zone NN5. These two zones overlap at ca. 13.6 Ma. Two Sr age estimates at 223.41 mcd have an average age of 14.5 Ma. The error bars on these age estimates plot within the biozones. The best correlation line for this sequence fit to the biostratigraphic data gives an age of 13.7–13.6 Ma (Fig. 4).

At Site M28, sequence m5 (276.81–254.23 mcd) is in ECDZ 6a and Zone NN5 as it is at Site M27; 21 Sr values obtained from this sequence have an average age of 14.3 Ma (an age estimate of 29.3 Ma at 254.18 mcd is interpreted as altered), 0.9 m.y. older than the biostratigraphic age estimates. However, the Sr isotopic data show considerable scatter (15.2–12.2 Ma), suggesting possible reworking of older material into this sequence. The best correlation line for this sequence based on the biostratigraphic data gives an age of 13.7–13.5 Ma (Fig. 5).

At Site M29, sequence m5 (502.01–478.61 mcd) is also in Zone NN5, as it is at M27 and M28; it is also assigned to Zone DN5 and ECDZ 5. A correlation line fit through all of the biostratigraphic markers gives an age of 13.7–13.6 Ma (Fig. 6).

Sequence m4.5

At Site M27, sequence m4.5 (218.39–209 mcd) is assigned to ECDZ 6a at the base and ECDZ 6b (i.e., older than 13 Ma) at the top, to Zone NN5 at the base and Zones NN6–NN7 undifferentiated (i.e., younger than 13.5 Ma) at the top, and Zone DN5b. Sr age estimates are

scattered (13.8–12.0 Ma), but are compatible with the biostratigraphy. The sequence is best dated as 13.5–13.2 Ma.

At Site M28, sequence m4.5 (254.23–243 mcd) is in Zone NN5 to possibly Zone NN6 at the upper boundary and to ECDZ 6b and Zone DN6. The top of Zone NN5 is older than ECDZ 6b and Zone DN6. Twenty-one Sr age estimates range from 16.0 to 10.7 Ma (average 13.8 Ma). The wide scatter in the data suggests there is either substantial alteration to the Sr values and/or reworking of older material. The sequence is dated as ca. 13.3–13.2 Ma based on diatom biostratigraphy, although the calcareous nannoplankton suggest that it is older than 13.5 Ma (Fig. 5).

At Site M29, sequence m4.5 (478.61–408.65 mcd) is in Zones NN5, ECDZ 6a, and DN5b. If the diatoms are reliably calibrated, the sequence has an age of 13.6–13.3 Ma. However, the dinocyst and calcareous nannoplankton data suggest that the sequence might be older (possibly 14.1–13.6 Ma) (Fig. 6), although this this could also be attributed to reworking of *Sphenolithus heteromorphus*.

Sequence m4.4

The m4.4 to m4.1 sequences are only dated at Site M29. Sequence m4.4 (409.27–377.15 mcd) has diatoms assigned to ECDZ 6a–ECDZ 6b undifferentiated. This is the same zone that is found in sequences m5 (below) and m4.3 and lower m4.2 (above). This indicates that the interval 478.61–364.86 mcd (>113 m) was deposited between 13.6 and 13.0 Ma (188 m/m.y.). However, calcareous nannoplankton are assigned to Zone NN5 (14.9–13.5 Ma). These zones have very little overlap in time. The sequence is assigned to dinocyst Zone DN5b, which overlaps both the calcareous nannoplankton and diatom zones. The sequence is constrained by the overlying and underlying sequences to have been deposited rapidly; if the diatoms are correctly calibrated, then the sequence was deposited between 13.3 and 13.2 Ma (plotted in Fig. 6). The calcareous nannoplankton suggest that the sequence is older (ca. 13.8–13.7 Ma). As in sequence m4.5, this could be due to potential reworking of the marker for the top of Zone NN5 (*Sphenolithus heteromorphus*).

Sequence m4.3

Biostratigraphic markers in sequence m4.3 (377.15–364.86 mcd) are the same as in underlying sequence m4.4. Three Sr age estimates (14.6, 14.4, and 14.9 Ma) are much older than the biostratigraphy. According to the diatom evidence, the sequence was deposited between 13.2 and 13.1 Ma (plotted in Fig. 6). The dinocysts and calcareous nannoplankton suggest that the sequence was deposited between 13.7 and 13.6 Ma.

Sequence m4.2

At Site M29, sequence m4.2 (364.86–342.81 mcd) is in upper Zone DN5b and Zone NN6; these two zones overlap between 13.5 and 13.2 Ma. It is also placed in ECDZ 6, with the topmost sample in ECDZ 7, which is 13.0 Ma at the base. Based on our line of correlation, this sequence is 13.1–13.0 Ma.

Sequence m4.1

Age relations in sequence m4.1 are too poorly constrained to allow the sequence to be reliably dated. Diatoms at Site M29 indicate that the lower part of the sequence is ECDZ 7 (13.0–12.6 Ma), and dinocysts are assigned to Zone DN6 (13.2–12.6 Ma). Extrapolation of sedimentation rates yields an age estimate of 13.0–12.7 Ma for the sequence, although the top of the sequence was not cored (Fig. 6).

Sequences Younger Than m4.1

Four seismic sequences above sequence m4.1 reach their maximum thickness on the middle continental shelf seaward of the Expedition 313 sites (m4, m3, m2, and m1 progressing upsection). Three of these can be seismically traced into Sites M27–M29, although they cannot be dated at Exp. 313 sites due to fluvial-estuarine environments (Miller et al., 2013b); however, they appear to be younger than ca. 12.7 Ma by superposition over sequence m4.1. This conflicts with age estimates originally assigned to m4 (older than 13.6 Ma) and m3 (13.6 Ma) dated on the slope (Miller et al., 1998), but these original time correlations require updating. We note the following revisions to the younger sequences: (1) sequence boundary m3 is within Chron C5An2 (12.3–11.9 Ma at Site 904); (2) sequence m2 is within range of *Globorotalia fohsi fohsi* at Site 904 (Snyder et al., 1996; older than 11.7 Ma), placing it within lower part of reversed magnetochron C5r.2r (12.0–11.6 Ma); and (3) sequence m1 is at or below the highest occurrence of *Paragloboratalia mayeri* in shelf wells (Greenlee et al., 1992; this taxon has its highest occurrence in mid-latitudes at the base of C5n [11.0 Ma; Miller et al., 1985] although in tropical latitudes it has a younger range [10.5 Ma; Wade et al., 2011]), and at Site 904, m1 is within the range of *Cyrtocapsella tetrapera* (Nigrini, 1996; with a highest occurrence of 11.8 Ma). Thus, we estimate ages of 12.6–12.4 Ma for sequence m4, 12.3–12.0 Ma for sequence m3, 12.0–11.8 Ma for sequence m2, and 11.8–11.4 Ma for sequence m1 (Fig. 6).

DISCUSSION

Correlation Among Sites

An important goal of Expedition 313 was to resolve the age relations of closely spaced (in time) Miocene sequences using integrated Sr isotopic stratigraphy and biostratigraphy. Because the three sites are connected on a seismic profile, there is high confidence in the physical correlation of the sequences. The age relations of the sequences found at the three sites are shown as high (solid colors) and low confidence (cross-hachured) in Figure 7. Sequences are sampled in one of three broad areas: (1) landward of the clinothem rollover in the topset (light blue in Fig. 7); (2) between the clinothem rollover and the lower clinothem break in slope on the foreset, where the sequence is thickest (medium blue in Fig. 7); and (3) seaward of the lower clinothem break in slope in the bottomset (dark blue in Fig. 7; see Mountain et al., 2010). In contrast to previous interpretations (Greenlee et al., 1992, Monteverde et al., 2008), foresets often contain thin LST, with thin TST, and thick HST (fig. 13 in Miller et al., 2013c). Sequences landward of the clinothem generally consist of stacked transgressive and highstand systems tracts, similar to what is found in the New Jersey coastal plain (Sugarman et al., 1993; Miller et al., 1997, 1998). Sequences in the bottomsets are dominated by sediment gravity-flow deposits (Mountain et al., 2010) and outer middle neritic muds (75–100 m paleodepth; Katz et al., 2013).

Age resolution of the sequences is variable. The poorest age resolution is obtained in sequences that were deposited during long biozones and that have long hiatuses above and below the sequence. Sequence m5.4 at M29 was deposited during Zones DN3 (18.2–16 Ma) and NN4 (17.9 and 14.9 Ma) with a hiatus of ~1.6 m.y. above. At Site M29, the resolution for sequence m5.4 is no better than ±1 m.y., but it is well dated (better than ±0.25 m.y.) at Site M27 by integrated stratigraphy (Fig. 7). The best resolution is obtained where sequences are deposited during short-ranging biozones, or where there is a change from one biozone to the next youngest zone within a sequence, and where there are short hiatuses above and below the sequence. Sequence m5.45 at Site M28 is in Zone NN4 and is also constrained by superposition to be older than 17.7 Ma. Sequence m5.2 at Site M28 was deposited where there is a change from diatom ECDZ 3–ECDZ 4 and nannofossil Zones NN4 to NN5. This requires the sequence to have been deposited during a narrow window of time (15.0–14.8 Ma) with a resolution of ~±0.25 m.y. The average resolution for the Miocene sequences at the 3 sites is ~±0.5 m.y.

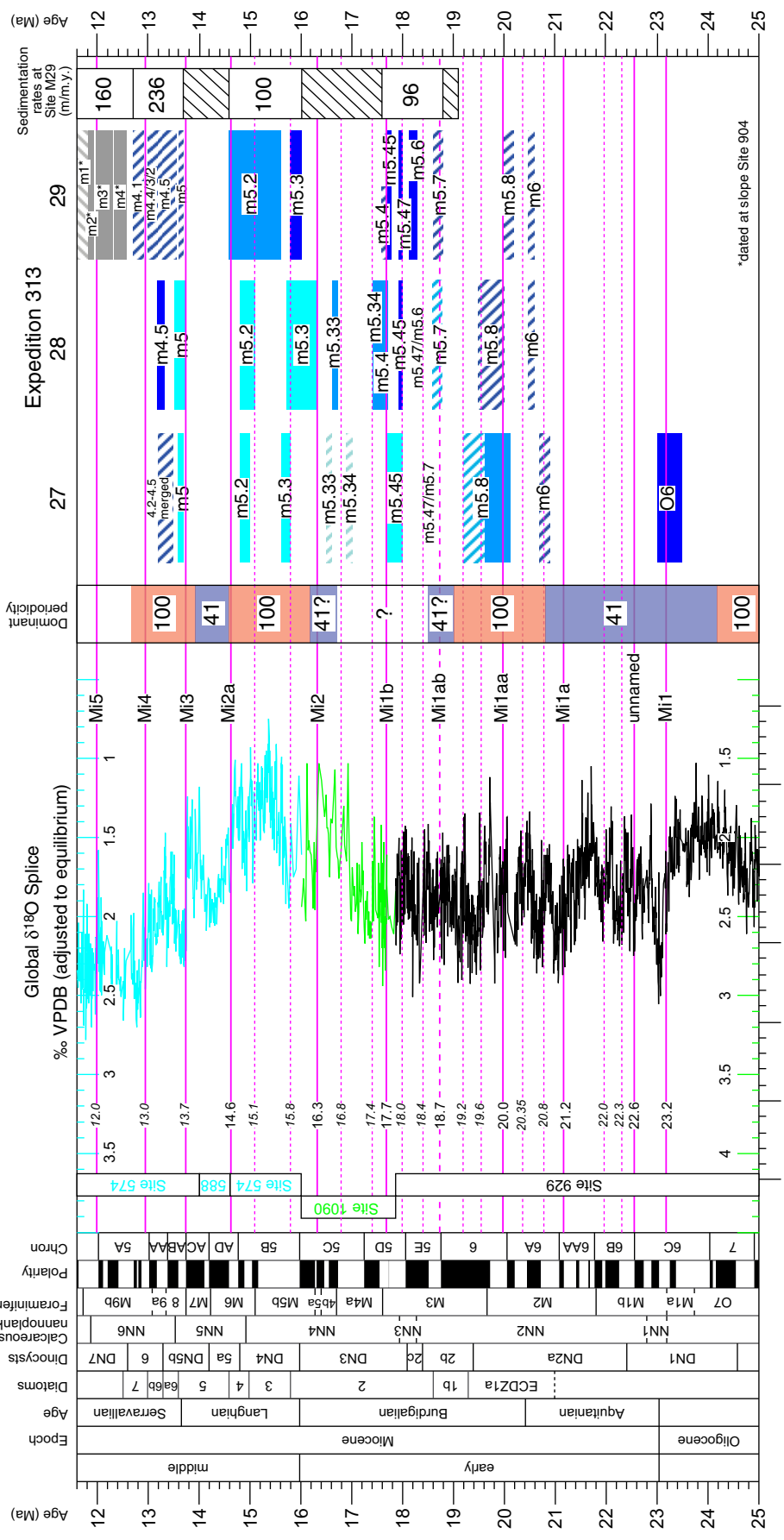

Figure 7. Colored blocks show time periods represented by Integrated Ocean Drilling Program Expedition 313 coreholes compared to the global oxygen isotopic record. Note that Oligocene sequences at Site M27 are not included here. Time scale of Gradstein et al. (2004); dinocyst calibration is after McCarthy et al. (2013) and diatom calibration is after Barron (2003). Corehole arranged from updip on left to downdip on right. Different colored blocks are used to show where the site is located with respect to the clinothem and the time represented by a given sequence (e.g., O6, m6). Medium blue is used to show the sequence was drilled through the thickest part of the sequence. Dark blue indicates deposition on the clinothem bottomsets. Light blue indicates deposition landward of the clinothem. Cross-hachures indicate less certain age tuned to better dated records at other sites. Benthic foraminiferal oxygen isotopic records from Deep Sea Drilling Project Sites 574 (black) and 588 (black), and Ocean Drilling Program Sites 1090 (green) and 929 and 926 composite (blue) are discussed in the text. Note that the oxygen isotopic scales are shifted relative to one another. The asterisk for sequences m4–m1 indicates a new age interpretation versus Miller et al. (1998). VPDB—Vienna Peedee belemnite; ECDZ—East Coast Diatom Zones.

Most sequences can be dated to ±0.25 m.y. at one site at least.

Expedition 313 sequences are best dated on the foreset, where they are thickest (i.e., sequence m5.8 at Site M27, composite sequence m5.4 at Site M28, and sequence m5.2 at Site M29; Mountain et al., 2010). At other sites where the age relations are poorly constrained or lacking, the age estimates can be constrained by coeval sequences at better dated sites to improve our understanding. The sequences are of similar age across the three sites and the principles of superposition and sequence stratigraphy apply an additional age constraint, i.e., all sediments above a sequence boundary are younger than the sediments below the sequence boundary. Our age estimates of poorly dated sequences (Fig. 7) are done within the constraints of better dated ones.

Sediments landward of the clinothem rollover generally correlate with the youngest part of the sediments dated in the foreset. Sediments in the bottomsets generally correlate with the older part of the sediments dated in the foreset. This relationship is shown best in composite sequence m5.4, where the sediments in the topset at Site M27 (17–16.8 Ma) correlate with the upper portion of sequence m5.4 (higher order sequence m5.33), whereas the bottomsets at Site M29 correlate with the oldest part of sequence m5.4 (higher order sequence m5.34).

Preservation of only the younger part of sequences on topsets is also seen in sequence m5.2, where the clinoform rollover is at Site M29 (15.6–14.6 Ma), and Sites M27 and M28 are on topsets (Fig. 7). Sequence m5.2 at both Sites M27 (15.0–14.8 Ma) and M28 (15.0–14.8 Ma) correlates with the younger portion of the sequence as dated at Site M29 (15.6–14.6 Ma). The ages of sequence m5.8 at Sites M28 and M29 are too poorly resolved to determine whether this relationship holds in that sequence, although it appears to be older in the bottomset. The relationship is more complicated for sequence m5.3. The age of the topset is 15.8–15.6 Ma at Site M27 (Fig. 7). The age of sequence m5.3 at Site M28 is 16.3–15.7 Ma. Seismic profiles (Fig. 2) show that sequence m5.3 at Site M28 is an eroded foreset (Fig. 2). The age on the bottomset at Site M29 is 16.0–15.8 Ma. In this case, the oldest part of the foreset may be somewhat older than the bottomset sediments, although the topset and foreset record the youngest sediments.

The timing of sequences deposited between 21 and 18.5 Ma (sequences m6, m5.8, and m5.7) and between 18 and 14.5 Ma (sequences m5.4, m5.3, and m5.2) agrees well across the transect. Closely spaced sequences (sequences m5.6, m5.47, m5.45, and sequences m5 and younger) are more difficult to date and site to site correlation of the individual sequences is less certain.

Use of Integrated Stratigraphy

Our study illustrates the need to fully integrate multiple fossil groups and use independent means of chronology (e.g., Sr isotopic stratigraphy) in shallow-water environments. Sr isotopic stratigraphy works well in the Oligocene to earliest middle Miocene, but there is poor resolution in the later middle to late Miocene due to a low rate of global $^{87}Sr/^{86}Sr$ change. Sr isotopic stratigraphy also suffers from reworking of stratigraphically older material in the upper middle Miocene of Expedition 313. In addition, a number of Sr isotope age estimates are clearly discordant and must be attributed to diagenetic alteration. Each microfossil group has its own limitation. Planktonic foraminifera were not useful in zoning Expedition 313 because (1) the assemblages were dominated by juveniles and (2) the few adult specimens present often resulted in identification of datum levels by single specimens, a potentially hazardous situation. Nannofossil biostratigraphy proved to be the most useful in initial studies and is critical to this study, although a few intervals have particularly long zones (e.g., NP25, NN2, and to a lesser extent NN4) with few additional bioevents within the zones to allow for increased resolution, at least within this shallow-water depositional environment. In contrast to previous diatom biostratigraphy on this margin that focused on large and predominantly benthic taxa, the use of planktonic diatoms that are well calibrated to the geological time scale proved to be an unexpected success and provided the best control in sediments younger than 15 Ma (Barron et al., 2013). However, there are still minor problems with the calibrations between diatoms and nannofossils and Sr isotope stratigraphy particularly in the early Miocene (e.g., ECDZ 1). Dinocysts provided useful constraints and were crucial in intervals lacking carbonate, although calibrations to the time scale are still uncertain. Despite these limitations, we were able to construct a reliable, reproducible chronology for these shallow-water deposits by integrating Sr isotopic stratigraphy with the three fossil groups, aided by a sequence stratigraphic framework that provided physical constraints in intercorehole correlations.

Sedimentation Rates

Sedimentation rates are difficult to compare among the three sites. Correlation lines (Fig. 4–6) through the age control points provide sedimentation rates, but have large enough errors on them as to make comparisons of rates within individual sequences difficult to interpret. However, differences can be compared by averaging sedimentation rates across several sequences, taking the total thickness divided by total time (including short hiatuses), thus providing minimum rates. Beginning at 13.7 Ma at Site M29 the average amount of sediment preserved per million years increased (1) from 18.3 to 17.6 (sequences m5.6, m5.47, m5.45, m5.4), 67 m are preserved (96 m/m.y. minimum rate); (2) from 16.0 to 14.6 Ma (sequences m5.3 and m5.2), 141 m are preserved (100 m/m.y.); (3) from 13.7 to 12.6 Ma (sequences m5, m4.5, m4.4, m4.3, m4.2, m4.1), 260 m are preserved (236 m/m.y.); and (4) from 12.6 to 11.4 Ma (sequences m4, m3, m2, and m1), 192 m are preserved (160 m/m.y.).

It is interesting that high sedimentation rates for sequences m4, m3, m2, and m1 are from sediments deposited on the topsets. Our study establishes that the dramatic increase in sediment accumulation (>2 fold) occurred between 14.6 and 13.7 Ma. This influx of sediments has been previously documented as a major increase in middle Miocene sedimentation rates on this margin (Poag and Sevon, 1987; Pazzaglia and Gardner, 1994), though here we are able to date this change relatively precisely as 14.6-13.7 Ma for input onto the shelf (Fig. 7). This increase has been attributed to uplift in the hinterland (Poag and Sevon, 1987; Pazzaglia and Gardner, 1994) and to middle Miocene climate changes (Steckler et al., 1999) associated with the development of a permanent East Antarctic Ice Sheet (EAIS) at 14.6–13.0 Ma and benthic foraminiferal $\delta^{18}O$ increases Mi2a, Mi3, and Mi4 (Fig. 7; Miller et al., 1991b). Here, we show that the increase in sedimentation rates is coincident with development of a permanent EAIS, strengthening the link between climate and sedimentation.

Sedimentation rates appear to be higher in the foreset beds than they are in the topset beds; bottomsets appear to have high rates also, but not as high as foresets. For the interval 18–14.8 Ma (sequences m5.45, m5.4, m5.3, and 5.2) topset beds are 136 m thick at Site M27, for a minimum rate of 43 m/m.y. Topsets for 16.3–14.8 Ma (sequences 5.3 and 5.2) are 84 m thick at Site M28, yielding a minimum rate of 56 m/m.y. In contrast, the m5.4 foreset (17.7–16.5 Ma; Site M28) accumulated 151 m in ~1.1 m.y. (138 m/m.y.). Two other foresets were sampled (m5.8 at Site M27 and m5.2 at Site M29); both had thick (134 and 100 m, respectively) accumulations in short intervals of time (~0.9 and 1 m.y.), yielding minimum rates of 150 and 100 m/m.y., respectively. Bottomsets

at Site M29 from 18.3 to 17.6 Ma (sequences m5.6, m5.47, m5.45, m5.4) accumulated 67 m, yielding a minimum rate of 95 m/m.y.

Correlative Conformity

We see no evidence for a correlative conformity in the time domain at Expedition 313 coreholes. We interpret that sequence boundaries are associated with hiatuses in nearly all cases older than 14 Ma (Fig. 7). Sequences m5.6 to m5.4 at Site 29, deposited in bottomsets, are too closely spaced in time for us to clearly resolve hiatuses, although there are physical unconformities that separate these sequences (Miller et al., 2013b). Sequences younger than 14 Ma were deposited in a short interval (more than 8 sequences in <2 m.y.) and possible hiatuses are shorter than our time resolution, although seismic stratigraphy indicates there are sequence boundaries (e.g., there are numerous sequence boundaries noted seaward of Expedition 313 that merge between sequence boundaries m4.1, m4, m3, and m2; Karakaya, 2012).

Correlation with $\delta^{18}O$ Record

Large continental ice sheets grew and decayed in Antarctica during the early to early-middle Miocene (e.g., Barrett et al., 1987; Miller et al., 1991b; Zachos et al., 2001). Although Northern Hemisphere ice existed at that time (Wolf-Welling et al., 1996; Wright and Miller, 1996), it was likely restricted to Greenland and mountain glaciers. The development of a large, permanent East Antarctic Ice Sheet (EAIS) in the middle Miocene (ca. 14.6–13.0 Ma) was associated with benthic foraminiferal $\delta^{18}O$ increases Mi2a, Mi3, and Mi4 (Fig. 7; e.g., Miller et al., 1991b). Waxing and waning of the Antarctica ice sheet during the Miocene caused large (tens of meters) changes in global sea level, leading to significant changes in accommodation on continental shelves. As sea level rises, increased accommodation allows the deposition and preservation of sequences (Vail et al., 1977, Posamentier et al., 1988). As sea level falls, decreases in accommodation caused downward shifts in base level and the formation of unconformities on the shelf.

Ice volume and attendant glacioeustatic changes cause global changes in $\delta^{18}O_{seawater}$ that are recorded in deep-sea benthic foraminiferal $\delta^{18}O$ records. Growing ice sheets sequester ^{16}O, causing the oceans to become enriched in ^{18}O. As ice sheets melt, sea level rises, and ^{16}O preferentially stored in ice is returned to the ocean. These changes have been measured in the world's ocean in deep-sea benthic foraminiferal $\delta^{18}O$ records, although these also reflect changes in deep ocean temperature and cannot be read as a strict ice-volume record (Fig. 7). Nevertheless, it is clear that a significant component of the Miocene $\delta^{18}O$ increases (e.g., Mi1, Mi1a) can be attributed to ice-volume increases (Lear et al., 2010).

We show time series of published deep-sea benthic foraminiferal $\delta^{18}O$ records and compare these to the Expedition 313 sequences (Fig. 7). The composite $\delta^{18}O$ record from Ceara Rise ODP Site 929 (black, Fig. 7; Zachos et al., 1996; Pälike et al., 2006) was sampled at 5 k.y. or better intervals. It extends from 25.0 to 17.86 Ma and (1) resolves the million-year-scale Mi1 and Mi1a oxygen isotopic increases and maxima (Miller et al., 1991b; Wright and Miller, 1992); (2) resolves an unnamed increase at 22.6 Ma (Boulila et al., 2011) (Fig. 7; note that we place magenta lines here at the inflections of the $\delta^{18}O$ increases; this differs from the original definition which is the maximum $\delta^{18}O$ value following the increase); (3) resolves million-year-scale increases Mi1aa (ca. 20 Ma), and Mi1b (17.7 Ma), first identified in low-resolution records (Wright and Miller, 1992; Miller et al., 1991b, 1998), although these are less obvious than the larger (~0.5‰–1.0‰) Mi1 and Mi1a increases; and (4) appears to record the Mi1ab (ca. 18.7 Ma) $\delta^{18}O$ increase reported from lower resolution records, although this is less certain.

Oxygen isotopic records for the interval from 17.86 to 16 Ma lack high-resolution sampling except for Southern Ocean ODP Site 1090 (Billups et al., 2002). This record shows considerably more variability than the overlapping portions of the Site 929 record (the Supplemental Figure[1] reproduces Fig. 7 with an overlay of the Site 1090 data over the Site 929 data, illustrating the high variability in the Site 1090 record). Nevertheless, the Site 1090 record provides resolution of the Mi2 $\delta^{18}O$ increase (ca. 16.3 Ma) and appears to capture Mi1b (17.7 Ma), observed in low-resolution records (Wright and Miller, 1992).

The middle to late Miocene, younger than 15.8 Ma, has excellent stable isotopic records: here we show a splice of high-resolution (typically 5 k.y. sampling) records from equatorial Pacific DSDP Site 574 (Pisias et al., 1985; 10.642–14.006 Ma and 14.6–16.0 Ma) and southwest Pacific DSDP Site 588 (Kennett, 1986; 14.029–14.642 Ma). These records show million-year-scale $\delta^{18}O$ variability associated with the early-middle Miocene buildup of a permanent EAIS (Mi2a, Mi3, and Mi4; Fig. 7) and the late-middle Miocene (Mi5).

We also tentatively identify 400-k.y.-scale $\delta^{18}O$ increases (shown as dashed lines in Fig. 7) between ca. 22.3 and 15.1 Ma. These increases are speculative in that they have not been validated in multiple records.

We compare the timing of Expedition 313 sequences to $\delta^{18}O$ changes (Fig. 7). Major million year inflections (Mi events) in the record are shown as magenta horizontal lines. Smaller 400 k.y. changes in the isotopic record are shown as dashed magenta lines. Generally, the timing and number of major Mi isotopic inflections that must in part reflect glacioeustatic lowerings correspond with sequence boundaries or hiatuses.

1. Mi1, the unnamed 23.6 Ma event, and Mi1a correspond with a long hiatus.
2. Mi1a and Mi1aa bracket sequence m6.
3. Mi1aa corresponds with the basal sequence boundary of sequence m5.8; although the poorly dated bottomset at Site M29 appears to predate the inflection and the age at Site M27 slightly predates it, these 200 k.y. discrepancies are well within our age control.
4. Mi1ab appears to correlate with the basal sequence boundary of sequence m5.7, although this sequence is poorly dated.
5. Mi1b corresponds with the basal sequence boundary of sequence m5.4.
6. Mi2 appears to correspond with the basal sequence boundary of sequence m5.3.
7. Mi2a corresponds with a hiatus (14.6–13.7 Ma).
8. Mi3 corresponds with the basal sequence boundary of sequence m5.
9. Mi4 corresponds with the basal sequence boundary of sequence m4.1.
10. Mi5 corresponds with the basal sequence boundary of sequence m2.

There are some exceptions to the correspondences between $\delta^{18}O$ increases and sequence boundaries.

1. Sequence O6, found only at Site M27, was deposited across the calcareous nannoplankton Zone NP25-NN1 boundary and appears to straddle the Mi1 $\delta^{18}O$ increase. However, dating of the sequence is too coarse to be definitive. The sea-level lowering associated with the Mi1 $\delta^{18}O$ increase is probably responsible for the O6 sequence boundary.
2. Sequence boundaries m5.7, m5.6, m5.47, and m5.45 were all deposited between 18.7 and 17.7 Ma, bracketed by $\delta^{18}O$ increases Mi1ab and Mi1b. We speculate that these sequence boundaries reflect high-order (400 k.y. scale) increases observed in the $\delta^{18}O$ record. This speculative correlation would have m5.7, m5.6, m5.47, and m5.45 sequence boundaries match

[1]Supplemental Figure. Reproduction of Figure 7 with an overlay of Ocean Drilling Program (ODP) Site 1090 data over the ODP Site 926–929 composite. If you are viewing the PDF of this paper or reading it offline, please visit http://dx.doi.org/10.1130/GES00857.S1 or the full-text article on www.gsapubs.org to view the Supplemental Figure.

observed $\delta^{18}O$ increases at 19.2, 18.7, 18.4, and 18.0 Ma, respectively.

3. Higher order sequence boundaries m5.4, m5.34, and m5.33 may be related to 400 k.y. scale $\delta^{18}O$ increases ca. 17.4 and 16.8 Ma, although this strains our chronologic resolution.

4. There is no million-year-scale $\delta^{18}O$ increase associated with the m5.2 sequence boundary, which appears to be ~0.3 m.y. older than the large Mi2a $\delta^{18}O$ increase; this strains our chronologic resolution and we suggest that this sequence boundary in fact correlates with the Mi2a increase.

Studies of deep-sea benthic foraminiferal $\delta^{18}O$ records show intriguing changes in the dominant astronomical pacing during the Miocene. Analysis of Miocene $\delta^{18}O$ records shows that the dominant long period controlling early to early-middle Miocene glacioeustasy was the 1.2-m.y.-long tilt cycle (Boulila et al., 2011). On higher frequency scales, early to middle Miocene $\delta^{18}O$ records record several changes in pacemaker from eccentricity-dominated (100 and 405 k.y.) to tilt-dominated (41 k.y.) benthic foraminiferal $\delta^{18}O$ variations (Pälike et al., 2006; Holbourn et al., 2007), as illustrated in Figure 7. Much of the Aquitanian was dominated by the 41 k.y. tilt cycle (24–20.8 Ma; Pälike et al., 2006), an interval that lacks preservation of sequences from Expedition 313 (Fig. 7). A 100-k.y.-eccentricity–dominated world is identified in $\delta^{18}O$ records from 20.8 to 19.2 Ma (Pälike et al., 2006); this interval includes sequences m6 and m5.8. Oxygen isotopic records are not sufficient to document the dominant pacing of the interval from 18.5 to 16.6 Ma, an interval that is well represented by 5 sequences. A return to 100-k.y.-eccentricity dominance from 16.2 to 14.6 Ma is indicated by $\delta^{18}O$ variations (Holbourn et al., 2007); this world was associated with preservation of sequences m5.3 and m5.2. In contrast, $\delta^{18}O$ variations indicate a return to a 41-k.y.-eccentricity world from 14.6 to 13.8 Ma (Holbourn et al., 2007); this is a major hiatus (Fig. 7). A return to another 100-k.y.-eccentricity world is indicated by $\delta^{18}O$ variations younger than 13.8 Ma. The 100-k.y.-eccentricity world has 5 sequences preserved in an ~0.7 m.y. interval. We speculate that sequences are differentially preserved during the 100-k.y.-eccentricity–dominated worlds but tend to be eroded away during the 41-k.y.-eccentricity–dominated worlds. This intriguing observation of differential preservation of sequences during intervals of different pacing requires further testing from other margins.

Sequences m5, m4.5, m4.4, m4.3, and m4.2 are all closely spaced sequences with high sedimentation rates (i.e., they were deposited between ca. 13.7 and 13.0 Ma, bracketed by the Mi3 and Mi4 $\delta^{18}O$ increases; Fig. 7). We speculate that these sequence boundaries may reflect 100-k.y.-eccentricity variability documented in the $\delta^{18}O$ record (Holbourn et al., 2007), but correlation to 100 k.y. pacing is beyond our age resolution.

CONCLUSION

We successfully dated the sequences from IODP Expedition 313 using integrated biostratigraphy and Sr isotopic stratigraphy. Sequences are most accurately dated where they are thickest and contain deeper water sediments. Sequences that were drilled in topsets or in bottomsets generally contain fewer fossils and cannot be dated as precisely. Sufficient material for dating is usually available in each sequence to confirm that the sequences are the same from one part of the seismic line to another, but in the absence of seismic stratigraphy, it would be difficult to unequivocally establish equivalency between these units using just the dating techniques available.

Although each individual sequence could not be dated at each corehole, age estimates of the less well-dated sequences are constrained by the better dated ones to establish a chronology for each corehole. These data, combined with water depth data, will be used for backstripping to construct a sea-level curve for this area.

The cause of the sequence boundaries is generally inferred to be sea-level change due to waxing and waning ice sheets in Antarctica. The Miocene sequences recovered by Expedition 313 were deposited during the early Miocene climate optimum (m5.8–m5.2) and the middle Miocene climate transition (m5–m4.2) that resulted in development of a permanent EAIS (Holbourn et al., 2007). Sedimentation rates were generally very high at Expedition 313 sites, consistent with rates first noted for this region by Poag and Sevon (1989), and we link this increase in sediment input to global climate changes associated with development of a permanent EAIS. The sedimentation rates increased in the middle Miocene at Site M29, in agreement with previous studies (Poag and Sevon, 1989; Steckler et al., 1999). The $\delta^{18}O$ proxy for ice-volume change records several large changes during this interval that are defined as the Mi events. Between these major events there are 400 and 100 k.y. shifts in the $\delta^{18}O$ record. In general there is a correlation between the timing and number of major isotopic inflections and sequence boundaries. This suggests that ice-volume changes, the primary driver of sea-level changes, may be the primary control on sedimentation patterns on the continental shelf. The data further suggest that sequences are more likely to be preserved during the 100-k.y.-eccentricity–dominated sea-level cycles, but are more likely to be eroded away during the 41-k.y.-eccentricity–dominated cycles.

ACKNOWLEDGMENTS

We thank the drillers and scientists of Integrated Ocean Drilling Program (IODP) Expedition 313 for their enthusiastic collaboration. We also thank the co-chief scientists, G. Mountain and J.-N. Proust, who helped with all aspects of drilling and data collection; U. Röhl and the staff of the Bremen Core Repository for hosting the onshore science party; J. Wright for discussion of Miocene climate; and C. Lombardi and J. Criscione for help preparing and analyzing samples. Funding was supplied by the U.S. Science Support Program Consortium for Ocean Leadership (COL/USSP) and samples were provided by the IODP and the International Continental Scientific Drilling Program (ICDP). We thank L. Edwards and two anonymous reviewers for reviews.

REFERENCES CITED

Andrews, G.W., 1988, A revised marine diatom zonation for Miocene strata of the southeastern United States: U.S. Geological Survey Professional Paper 1481, 29 p.

Austin, J.A., Christie-Blick, N., Malone, M., and the Leg 174A Shipboard Party, 1998, Proceedings of the Ocean Drilling Program, Initial reports, Volume 174A: College Station, Texas, Ocean Drilling Program, 324 p., doi:10.2973/odp.proc.ir.174a.1998.

Barrett, P.J., Elston, D.P., Harwood, D.M., McKeley, B.C., and Webb, P.N., 1987, Mid-Cenozoic record of glaciation and sea-level change on the margin of the Victoria Land Basin, Antarctica: Geology, v. 15, p. 634–637, doi:10.1130/0091-7613(1987)15<634:MROGAS>2.0.CO;2.

Barron, J.A., 2003, Appearance and extinction of planktonic diatoms during the past 18 m.y. in the Pacific and Southern Oceans: Diatom Research, v. 18, p. 203–224, doi:10.1080/0269249X.2003.9705588.

Barron, J., Browning, J.V., Sugarman, P.J., and Miller, K.G., 2013, Refinement of late-Early and Middle Miocene diatom biostratigraphy for the East Coast of the United States: Geosphere, v. 9, doi:10.1130/GES00864.1.

Berggren, W.A., Kent, D.V., Swisher, C.C., III, and Aubry, M.-P., 1995, A revised Cenozoic geochronology and chronostratigraphy, *in* Berggren, W.A., et al., eds., Geochronology, time scales and global stratigraphic correlations: SEPM (Society for Sedimentary Geology) Special Publication 54, p. 129–212, doi:10.2110/pec.95.04.0129.

Billups, K., Channell, J.E.T., and Zachos, J.C., 2002, Late Oligocene to early Miocene geochronology and paleoceanography from the subantarctic South Atlantic: Paleoceanography, v. 17, p. 4-1–4-11, doi:10.1029/2000PA000568.

Boulila, S., Galbrun, B., Miller, K.G., Pekar, S.F., Browning, J.V., Laskar, J., and Wright, J.D., 2011, On the origin of Cenozoic and Mesozoic "third-order" eustatic sequences: Earth-Science Reviews, v. 109, p. 94–112, doi:10.1016/j.earscirev.2011.09.003.

Bown, P.R., ed., 1998, Calcareous nannofossil biostratigraphy: Cambridge, UK, Cambridge University Press, 328 p., doi:10.1007/978-94-011-4902-0.

Bown, P.R., and Young, J.R., 1998, Techniques, *in* Bown, P.R., ed., Calcareous nannofossil biostratigraphy: Cambridge, UK, Cambridge University Press, p. 16–28.

Broecker, W.S., and Peng, T.H., 1982, Tracers in the sea: Palisades, New York, Eldigio, 690 p.

Burke, W.H., Denison, R.E., Hetherington, E.A., Koepnick, R.B., Nelson, H.F., and Otto, J.B., 1982, Variation of seawater $^{87}Sr/^{86}Sr$ throughout Phanerozoic time: Geology, v. 10, p. 516–519, doi:10.1130/0091-7613(1982)10<516:VOSSTP>2.0.CO;2.

Cande, S.C., and Kent, D.V., 1995, Revised calibration of the geomagnetic polarity time scale for the Late Cretaceous and Cenozoic: Journal of Geophysical Research, v. 100, p. 6093–6095, doi:10.1029/94JB03098.

Christie-Blick, N., Mountain, G.S., and Miller, K.G., 1990, Seismic stratigraphic record of sea-level change, in Geophysics Study Committee, National Research Council, Sea-level change: National Academy of Sciences Studies in Geophysics: Washington, D.C., National Academy Press, p. 116–140.

de Verteuil, L., and Norris, G., 1996, Miocene dinoflagellate stratigraphy and systematics of Maryland and Virginia: Micropaleontology, v. 42, supplement, p. 1–172, doi:10.2307/1485926.

Dybkjaer, K., and Piasecki, S., 2008, A new Neogene biostratigraphy of Denmark: Geological Survey of Denmark and Greenland Bulletin, v. 15, p. 29–32.

Dybkjaer, K., and Piasecki, S., 2010, Neogene dinocyst zonation for the eastern North Sea Basin, Denmark: Review of Palaeobotany and Palynology, v. 161, p. 1–29, doi:10.1016/j.revpalbo.2010.02.005.

Embry, A.F., 2009, Practical sequence stratigraphy: Canadian Society of Petroleum Geologists, 81 p., www.cspg.org.

Expedition 313 Scientists, 2010a, Site M0027, *in* Mountain, G., et al., Proceedings of the Integrated Ocean Drilling Program 313: Tokyo, Integrated Ocean Drilling Program Management International, Inc., doi:10.2204/iodp.proc.313.103.2010

Expedition 313 Scientists, 2010b, Site M0028, *in* Mountain, G., et al., Proceedings of the Integrated Ocean Drilling Program 313: Tokyo, Integrated Ocean Drilling Program Management International, Inc., doi:10.2204/iodp.proc.313.104.2010

Expedition 313 Scientists, 2010c, Site M0029, *in* Mountain, G., et al., Proceedings of the Integrated Ocean Drilling Program 313: Tokyo, Integrated Ocean Drilling Program Management International, Inc., doi:10.2204/iodp.proc.313.105.2010

Expedition 313 Scientists, 2010d, Methods, *in* Mountain, G., et al., Proceedings of the Integrated Ocean Drilling Program 313: Tokyo, Integrated Ocean Drilling Program Management International, Inc., doi:10.2204/iodp.proc.313.102.2010.

Gradstein, F., Ogg, J., and Smith, A., 2004, A geologic time scale 2004: Cambridge, U.K., Cambridge University Press, 589 p.

Gradstein, F.M., Ogg, J.G., Schmidtz, M.D., and Ogg, G.M., eds., 2012, The geologic time scale: New York, Elsevier, 1144 p.

Greenlee, S.M., and Moore, T.C., 1988, Recognition and interpretation of depositional sequences and calculation of sea-level changes from stratigraphic data—Offshore New Jersey and Alabama Tertiary, *in* Wilgus, C.K., et al., eds., Sea-level changes: An integrated approach: Society of Economic Paleontologists and Mineralogists Special Publication 42, p. 329–353, doi:10.2110/pec.88.01.0329.

Greenlee, S.M., Devlin, W.J., Miller, K.G., Mountain, G.S., and Flemings, P.B., 1992, Integrated sequence stratigraphy of Neogene deposits, New Jersey continental shelf and slope: Comparison with the Exxon model: Geological Society of America Bulletin, v. 104, p. 1403–1411, doi:10.1130/0016-7606(1992)104<1403:ISSOND>2.3.CO;2.

Hart, S.R., and Brooks, C., 1974, Clinopyroxene-matrix partitioning of K, Rb, Cs, and Ba: Geochimica et Cosmochimica Acta, v. 38, p. 1799–1806, doi:10.1016/0016-7037(74)90163-X.

Hathaway, J.C., Poag, C.W., Valentine, P.C., Miller, R.E., Schultz, D.M., Manheim, R.T., Kohout, F.A., Bothner, M.H., and Sangrey, D.A., 1979, U.S. Geological Survey core drilling on the Atlantic shelf: Science, v. 206, p. 515–527, doi:10.1126/science.206.4418.515.

Hodell, D.A., Mead, G.A., and Mueller, P., 1990, Variations in the strontium isotopic composition of seawater (8 Ma to present): Implications for chemical weathering rates and dissolved fluxes to the oceans: Chemical Geology, v. 80, p. 291–307, doi:10.1016/0168-9622(90)90011-Z.

Holbourn, A.E., Kuhnt, W., Schulz, M., Flores, J.-A., and Andersen, N., 2007, Orbitally-paced climate evolution during the middle Miocene "Monterey" carbon-isotope excursion: Earth and Planetary Science Letters, v. 261, p. 534–550, doi:10.1016/j.epsl.2007.07.026.

Karakaya, S., 2012, Quantitative seismic attribute analysis using artificial neural networks and seismic stratigraphic interpretation of lower to middle Miocene sediments offshore New Jersey [M.S. thesis]: New Brunswick, New Jersey, Rutgers University, 190 p.

Katz, M.E., Browning, J.V., Miller, K.G., Monteverde, D., Mountain, G.S., and Williams, R.H., 2013, Paleobathymetry and sequence stratigraphic interpretations from benthic foraminifera: Insights on New Jersey shelf architecture, IODP Expedition 313: Geosphere, doi:10.1130/GES00872.1.

Kennett, J.P., 1986, Miocene to early Pliocene oxygen and carbon isotope stratigraphy in the southwest Pacific, Deep Sea Drilling Project Leg 90, *in* Kennett, J.P., et al., Initial reports of the Deep Sea Drilling Project, Volume 90: Washington, D.C., U.S. Government Printing Office, p. 1383–1411, doi:10.2973/dsdp.proc.90.142.1986.

Kominz, M.A., Browning, J.V., Miller, K.G., Sugarman, P.J., Misintseva, S., and Scotese, C.R., 2008, Late Cretaceous to Miocene sea-level estimates from the New Jersey and Delaware coastal plain coreholes: An error analysis: Basin Research, v. 20, p. 211–226, doi:10.1111/j.1365-2117.2008.00354.x.

Lear, C.H., Mawbey, E.M., and Rosenthal, Y., 2010, Cenozoic benthic foraminiferal Mg/Ca and Li/Ca records: Toward unlocking temperatures and saturation states: Paleoceanography, v. 25, PA4215, doi:10.1029/2009PA001880.

Martini, E., 1971, Standard Tertiary and Quaternary calcareous nannoplankton zonation, *in* Farinacci, A., ed., Proceedings of the Second International Conference on Planktonic Microfossils, Volume 2: Rome, Edizioni Tecnoscienza, p. 739–785.

McArthur, J.M., Howarth, R.J., and Bailey, T.R., 2001, Strontium isotope stratigraphy: LOWESS Version 3. Best-fit line to the marine Sr isotope curve for 0 to 509 Ma and accompanying look-up table for deriving numerical age: Journal of Geology, v. 109, p. 155–170, doi:10.1086/319243.

McCarthy, F.M.G., Katz, M.E., Kotthoff, U., Drljepan, M., Zanatta, R., Williams, R.H., Browning, J.V., Hesselbo, S.P., Bjerrum, C.J., Miller, K.G., and Mountain, G.S., 2013, Eustatic control of New Jersey margin architecture: Palynological evidence from IODP Expedition 313: Geosphere, doi:10.1130/GES00853.1.

Miller, K.G., Aubry, M.-P., Khan, J., Melillo, A.J., Kent, D.V., and Berggren, W.A., 1985, Oligocene–Miocene biostratigraphy, magnetostratigraphy, and isotopic stratigraphy of the western North Atlantic: Geology, v. 13, p. 257–261, doi:10.1130/0091-7613(1985)13<257:OBMAIS>2.0.CO;2.

Miller, K.G., Feigenson, M.D., Wright, J.D., and Clement, B.M., 1991a, Miocene isotope reference section, Deep Sea Drilling Project Site 608: An evaluation of isotope and biostratigraphic resolution: Paleoceanography, v. 6, p. 33–52, doi:10.1029/90PA01941.

Miller, K.G., Wright, J.D., and Fairbanks, R.G., 1991b, Unlocking the ice house: Oligocene–Miocene oxygen isotopes, eustasy, and margin erosion: Journal of Geophysical Research, v. 96, p. 6829–6848, doi:10.1029/90JB02015.

Miller, K.G., Mountain, G.S., the Leg 150 Shipboard Party, and Members of the New Jersey Coastal Plain Drilling Project, 1996, Drilling and dating New Jersey Oligocene–Miocene sequences: Ice volume, global sea level, and Exxon records: Science, v. 271, p. 1092–1095, doi:10.1126/science.271.5252.1092.

Miller, K.G., Rufolo, S., Sugarman, P.J., Pekar, S.F., Browning, J.V., and Gwynn, D.W., 1997, Early to middle Miocene sequences, systems tracts, and benthic foraminiferal biofacies, New Jersey coastal plain, *in* Miller, K.G., and Snyder, S.W., eds., Proceedings of the Ocean Drilling Program, Scientific results, Volume 150X: College Station, Texas, Ocean Drilling Program, p. 169–186, doi:10.2973/odp.proc.sr.150X.313.1997.

Miller, K.G., Mountain, G.S., Browning, J.V., Kominz, M., Sugarman, P.J., Christie-Blick, N., Katz, M.E., and Wright, J.D., 1998, Cenozoic global sea-level, sequences, and the New Jersey transect: Results from coastal plain and slope drilling: Reviews of Geophysics, v. 36, p. 569–601, doi:10.1029/98RG01624.

Miller, K.G., Browning, J.V., Sugarman, P.J., McLaughlin, P.P., Kominz, M.A., Olsson, R.K., Wright, J.D., Cramer, B.S., Pekar, S.F., and Van Sickel, W., 2003, 174AX leg summary: Sequences, sea level, tectonics, and aquifer resources: Coastal plain drilling, *in* Miller, K.G., et al., eds., Proceedings of the Ocean Drilling Program, Initial reports, Volume 174AX (supplement): College Station, Texas, Ocean Drilling Program, p. 1–38, doi:10.2973/odp.proc.ir.174axs.104.2003.

Miller, K.G., Kominz, M.A., Browning, J.V., Wright, J.D., Mountain, G.S., Katz, M.E., Sugarman, P.J., Cramer, B.S., Christie-Blick, N., and Pekar, S.F., 2005, The Phanerozoic record of global sea-level change: Science, v. 310, p. 1293–1298, doi:10.1126/science.1116412.

Miller, K.G., Sugarman, P.J., Browning, J.V., Sheridan, R.E., Kulhanek, D.K., Monteverde, D., Wehmiller, J.F., Lombardi, C., and Feigenson, M.D., 2013a, Pleistocene sequence stratigraphy of the shallow continental shelf, offshore New Jersey: Constraints of Integrated Ocean Drilling Program Leg 313 core holes: Geosphere, v. 9, p. 74–95, doi:10.1130/GES00795.1.

Miller, K.G., Browning, J.V., Mountain, G.S., Bassetti, M.A., Monteverde, D., Katz, M.E., Inwood, J., Lofi, J., and Proust, J.-N., 2013b, Sequence boundaries are impedance contrasts: Core-seismic-log integration of Oligocene–Miocene sequences, New Jersey shallow shelf: Geosphere, v. 9, doi:10.1130/GES00858.1.

Miller, K.G., and 13 others, 2013c, Testing sequence stratigraphic models by drilling Miocene foresets on the New Jersey shallow shelf: Geosphere, v. 9, doi:10.1130/GES00884.1.

Monteverde, D.H., 2008, Sequence stratigraphic analysis of early and middle Miocene shelf progradation along the New Jersey margin [Ph.D. thesis]: New Brunswick, New Jersey, Rutgers University, 247 p.

Monteverde, D.H., Mountain, G.S., and Miller, K.G., 2008, Early Miocene sequence development across the New Jersey margin: Basin Research, v. 20, p. 249–267, doi:10.1111/j.1365-2117.2008.00351.x.

Mountain, G.S., and Monteverde, D.H., 2012, If you've got the time, we've got the depth: The importance of accurate core-seismic correlation: American Geophysical Union Fall meeting, abstract PP51B-2111.

Mountain, G.S., Miller, K.G., Blum, P., Poag, C.W., and Twitchell, D.C., et al., 1996, Proceedings of the Ocean Drilling Program, Scientific results, Volume 150: College Station, Texas, Ocean Drilling Program, 885 p., doi:10.2973/odp.proc.ir.150.1994.

Mountain, G.S., Proust, J.-N., McInroy, D., Cotterill, C., and the Expedition 313 Scientists, 2010, Proceedings of the Integrated Ocean Drilling Program, Expedition 313: Tokyo, Integrated Ocean Drilling Program Management International, Inc., doi:10.2204/iodp.proc.313.2010.

Nigrini, C., 1996, Radiolarian biostratigraphy of Sites 902, 903, and 904, *in* Mountain, G.S., et al., eds., Proceedings of the Ocean Drilling Program, Scientific results, Volume 150: College Station, Texas, Ocean Drilling Program, p. 37–51, doi:10.2973/odp.proc.sr.150.006.1996.

Oslick, J.S., Miller, K.G., and Feigenson, M.D., 1994, Oligocene–Miocene strontium isotopes: Stratigraphic revisions and correlations to an inferred glacioeustatic record: Paleoceanography, v. 9, p. 427–443, doi:10.1029/94PA00249.

Pälike, H., Frazier, J., and Zachos, J.C., 2006, Extended orbitally forced palaeoclimatic records from the equatorial Atlantic Ceara Rise: Quaternary Science Reviews, v. 25, p. 3138–3149, doi:10.1016/j.quascirev.2006.02.011.

Pazzaglia, F.J., and Gardner, T.W., 1994, Late Cenozoic flexural deformation of the middle U.S. Atlantic passive margin: Journal of Geophysical Research, v. 99, p. 12,143–12,157, doi:10.1029/93JB03130.

Pekar, S.F., Christie-Blick, N., Kominz, M.A., and Miller, K.G., 2001, Evaluating the stratigraphic response to eustasy from Oligocene strata in New Jersey: Geology, v. 29, p. 55–58, doi:10.1130/0091-7613(2001)029<0055:ETSRTE>2.0.CO;2.

Perch-Nielsen, K., 1985, Cenozoic calcareous nannofossils, *in* Bolli, H.M., et al., eds., Plankton stratigraphy: Cambridge, UK, Cambridge University Press, p. 427–554.

Pisias, N.G., Shackleton, N.J., and Hall, M.A., 1985, Stable isotope and calcium carbonate records from hydraulic piston cored Hole 574A: High-resolution records from the middle Miocene, *in* Mayer, L., et al., Initial reports of the Deep Sea Drilling Project, Volume 85: Washington, D.C., U.S. Government Printing Office, p. 735–748, doi:10.2973/dsdp.proc.85.121.1985.

Poag, C.W., 1985, Depositional history and stratigraphic reference section for central Baltimore Canyon trough, *in* Poag, C.W. ed., Geologic evolution of the United States Atlantic Margin: New York, Van Nostrand Reinhold, p. 217–263.

Poag, C.W., and Sevon, W.D., 1989, A record of Appalachian denudation in postrift Mesozoic and Cenozoic sedimentary deposits of the U.S. middle Atlantic margin: Geomorphology, v. 2, p. 119–157, doi:10.1016/0169-555X(89)90009-3.

Posamentier, H.W., Jervey, M.T., and Vail, P.R., 1988, Eustatic controls on clastic deposition I—Conceptual framework, *in* Wilgus, C.K., et al., eds., Sea-level changes: An integrated approach: Society of Economic Paleontologists and Mineralogists Special Publication 42, p. 109–124, doi:10.2110/pec.88.01.0109.

Reilly, T.J., Miller, K.G., and Feigenson, M.D., 2002, Late Eocene to Oligocene Sr-isotopic reference section, Site 522, eastern South Atlantic: Paleoceanography, v. 18, p. 1–9.

Schlee, J.S., 1981, Seismic stratigraphy of Baltimore Canyon Trough: American Association of Petroleum Geologists Bulletin, v. 65, p. 26–53.

Snyder, S.W., Miller, K.G., and Saperson, E., 1996, Paleogene and Neogene planktonic foraminiferal biostratigraphy of the New Jersey continental slope: Sites 902, 903, and 904 (Leg 150), *in* Mountain, G.S., et al., eds., Proceedings of the Ocean Drilling Program, Scientific results, Volume 150: College Station, Texas, Ocean Drilling Program, p. 3–15, doi:10.2973/odp.proc.sr.150.001.1996.

Steckler, M.S., Mountain, G.S., Miller, K.G., and Christie-Blick, N., 1999, Reconstruction of Tertiary progradation and clinoform development on the New Jersey passive margin by 2-D backstripping: Marine Geology, v. 154, p. 399–420, doi:10.1016/S0025-3227(98)00126-1.

Sugarman, P.J., Miller, K.G., Owens, J.P., and Feigenson, M.D., 1993, Strontium-isotope and sequence stratigraphy of the Miocene Kirkwood Formation, southern New Jersey: Geological Society of America Bulletin, v. 105, p. 423–436, doi:10.1130/0016-7606(1993)105<0423:SIASSO>2.3.CO;2.

Sugarman, P.J., Miller, K.G., Bukry, D., and Feigenson, M.D., 1995, Uppermost Campanian–Maestrichtian strontium isotopic, biostratigraphic, and sequence stratigraphic framework of the New Jersey Coastal Plain: Geological Society of America Bulletin, v. 107, p. 19–37, doi:10.1130/0016-7606(1995)107<0019:UCMSIB>2.3.CO;2.

Vail, P.R., Mitchum, R.M., Jr., Todd, R.G., Widmier, J.M., Thompson, S., III, Sangree, J.B., Bubb, J.N., and Hatlelid, W.G., 1977, Seismic stratigraphy and global changes of sea level, *in* Payton, C.E., ed., Seismic stratigraphy—Applications to hydrocarbon exploration: American Association of Petroleum Geologists Memoir 26, p. 49–212.

Wade, B.S., Pearson, P.N., Berggren, W.A., and Pälike, H., 2011, Review and revision of Cenozoic tropical planktonic foraminiferal biostratigraphy and calibration to the geomagnetic polarity and astronomical time scale: Earth-Science Reviews, v. 104, p. 111–142, doi:10.1016/j.earscirev.2010.09.003.

Wolf-Welling, T.C.W., Cremer, M., O'Connell, S., Winkler, A., and Thiede, J., 1996, Cenozoic Arctic gateway paleoclimate variability: Indications from changes in coarse-fraction composition, *in* Thiede, J., et al., eds., Proceeding of the Ocean Drilling Program, Scientific results, Volume 151, p. 515–567, doi:10.2973/odp.proc.sr.151.139.1996.

Wright, J.D., and Miller, K.G., 1992, Miocene stable isotope stratigraphy, Site 747, Kerguelen Plateau, *in* Wise, S.W., Jr., et al., Proceedings of the Ocean Drilling Program, Scientific results, Volume 120, Part B: College Station, Texas, Ocean Drilling Program, p. 855–866, doi:10.2973/odp.proc.sr.120.193.1992.

Wright, J.D., and Miller, K.G., 1996, Control of North Atlantic deep water circulation by the Greenland-Scotland Ridge: Paleoceanography, v. 11, p. 157–170, doi:10.1029/95PA03696.

Zachos, J.C., Quinn, T.M., and Salamy, S., 1996, High resolution (10^4 yr) deep-sea foraminiferal stable isotope records of the earliest Oligocene climate transition: Paleoceanography, v. 11, p. 251–266, doi:10.1029/93PA03266.

Zachos, J.C., Shackleton, N., Revenaugh, J., Pälike, H., and Flower, B., 2001, Climate response to orbital forcing across the Oligocene-Miocene boundary: Science, v. 292, p. 274–278, doi:10.1126/science.1058288.